Physics – Uspekhi **67** (1) 22 – 43 (2024)

REVIEWS OF TOPICAL PROBLEMS

PACS numbers: **05.40. – a**, 05.70.Fh, **05.90. + m**, 61.05.fg, **71.27. + a**, 75.20.Ck, 75.20.En, 75.25.Dk, 75.30.Kz, 75.47.Np, 75.50.Pp, **76.30. – v**

Spin-fluctuation transitions

S V Demishev

DOI: https://doi.org/10.3367/UFNe.2023.05.039363

Contents

Abstract. Spin-fluctuation transitions (SFTs) are generally understood as a change in the characteristics of spin fluctuations in a magnet under the effect of control parameters (for example, temperature or composition of the material), not directly related to the formation of phases with long-range magnetic order. Therefore, SFTs in most cases go beyond the standard theory of phase transitions, where fluctuations are typically considered a phenomenon accompanying a magnetic transition. We examine the current state of the SFT issue from the theoretical and experimental standpoints, including the example of MnSi and $\mathbf{Mn_{1-x}Fe_xSi}$ helical magnets, $\mathbf{Hg_{1-x}Mn_xTe}$ magnetic semiconductors, doped compensated Ge:As(Ga) semiconductors, and a strongly correlated metal with hidden order, $\mathbf{CeB_6}$. The main methods for studying SFTs (neutron scattering and electron paramagnetic resonance) are discussed. We consider SFTs in the spin nematic phase, Ising disordered systems, paramagnetic and magnetically ordered phases, and quantum critical systems, as well as SFTs caused by changes in the spin dynamics. In discussing the SFT issue, we use the spin-polaron model, which unites objects of study that look disparate at first glance. We note that SFTs have not been studied in sufficient detail, and further research in this area may be one of the growth points in the modern physics of magnetic phenomena.

Keywords: magnetic phenomena, spin-fluctuation transitions, spin fluctuations, spin polarons, spin nematics, systems with hidden order, quantum critical systems, helical magnets, neutron scattering, electron paramagnetic resonance, MnSi, $Mn_{1-x}Fe_xSi$, $Hg_{1-x}Mn_xTe$, Ge:As(Ga), CeB_6

S V Demishev [1, 2, 3]
[1] Vereshchagin Institute for High Pressure Physics, Russian Academy of Sciences, Kaluzhskoe shosse 14, 108840 Troitsk, Moscow, Russian Federation
[2] Prokhorov General Physics Institute, Russian Academy of Sciences, ul. Vavilova 38, 119991 Moscow, Russian Federation
[3] National Research University Higher School of Economics, ul. Myasnitskaya 20, 101000 Moscow, Russian Federation
E-mail: demishev@hppi.troitsk.ru

Received 19 January 2023, revised 15 April 2023
Uspekhi Fizicheskikh Nauk **194** (1) 23 – 47 (2024)
Translated by S Alekseev

1. Introduction

Classifying magnetic phase transitions cannot be considered an altogether rewarding scientific task. On the one hand, magnetic phases can easily be classified according to the type of magnetic response, which divides them into two groups, paramagnetic and diamagnetic. However, the most interesting physical effects are then overlooked, and therefore the classification has to be made more intricate by considering the types of magnetic interactions and the corresponding magnetic structures. A classic case is extending the systematics to include magnetically ordered phases such as ferromagnets, antiferromagnets, and ferrimagnets [1]. Because phases with magnetic order are formed at certain values of external parameters, the paramagnetic phase, which has no long-range magnetic order, has to be made part of the 'standard picture.' The transition from magnetic order to magnetic disorder is accompanied by symmetry changes, suggesting that a suitable tool could be provided by the Landau theory [2–5], where the order parameters can be chosen as the sample magnetization, the sublattice magnetization, or their combination.

From the standpoint of the modern physics of magnetic phenomena, the above list of phases is clearly incomplete. In

the case of localized magnetic moments, it must be supplemented with a helical phase and a spin-glass phase. For systems with nonlocalized magnetic moments (distributed spin density), itinerant ferromagnets and antiferromagnets must be included. The magnetism of band electrons introduces a spin density wave phase and a superconducting phase. Furthermore, we should not forget about magnetically 'exotic' cases, including systems with hidden (quadrupole) order, spin liquids, dimerized, and spin-Peierls phases, nontrivial spin textures, and skyrmion phases. The landscape of magnetic phase transitions is further enriched with changes in dimension and with quantum phase transitions. Of course, the range of magnetic phases and phase transitions mentioned above is not exhaustive, and as the physics of magnetic phenomena develops, new objects keep appearing. On the other hand, complicating any classification scheme by including various larger or smaller details would undermine its usability.

Although magnetic phase transitions sometimes play the role of model objects in the physics of phase transitions [4–6], the terms 'phase' and 'phase transition,' borrowed from thermodynamics, are not necessarily understood fully rigorously in the field of magnetic phenomena. On the one hand, it was noted in [7] that the ''special power of imagination is required to discern a physical analogy between spontaneous magnetization associated with the ordering of elementary magnetic moments along a certain direction and the two-phase gas–liquid state.'' On the other hand, interfaces, equations of state, chemical potentials, and thermodynamic variables and their derivatives, which are certainly important in the thermodynamic description of gas–liquid or liquid–solid transitions [2, 7], do not always manifest themselves in the problems of magnetic phase transitions. In addition, magnetic phase transitions, in and of themselves, amount to a change in the magnetic properties of solids, which entails the problem (which is not always recognized) of the applicability of statistical mechanics [8]. As is well known, the antiferromagnetic phase, which is quite 'respectable' in the physics of magnetic phenomena, cannot be regarded as the ground state [1]. Admittedly, classical statistical physics also has its own 'bottlenecks,' in particular, the problem of extending the general systematics to metastable phases [9], which in practical terms are no less real than ideal thermodynamic phases. Phenomena that are not entirely canonical are also known, such as phase transitions in liquids [10, 11], with long-range order absent on both sides of the transition. Liquid crystals are in a class of their own, where, for example, in describing the simplest case of an isotropic liquid–nematic transition, the order parameter is given by one of the coefficients of the expansion in Legendre polynomials of the angular orientation distribution function of molecules [12, 13].

An excursion into the field of phase transitions cannot be complete without mentioning fluctuation problems. In the vicinity of the transition temperature, it is always possible to identify a region in which fluctuations play a significant role and can result in a divergence of physical quantities. The modern view of the problem of the fluctuation region implies a universal description. If the theory involves power-law divergences, then universality can be seen both in the values of critical exponents and in the relations between them, which often depend very weakly on the type of experimental system undergoing a phase transition [7, 14, 15]. Another option for describing the singularity is a logarithmic divergence at the transition point, which is obtained theoretically for some model systems [7] and, by definition, is universal and does not require discussing the problem of phase transitions in terms of critical exponents. There is also a version of the theory that predicts not just power-law singularities [4]. Interestingly, from the experimental standpoint, it may be almost impossible in some cases to distinguish between logarithmic and power-law singularities [16], and the interpretation of the data may therefore become model dependent.

We have tried to note some features of the paradigm within which various phase transitions are typically described, by no means claiming completeness or rigor of the presentation. It is apparently important that, as befits a paradigm, it aspire to give a universal and comprehensive description. We see, however, that there are several exceptions to the universal rules, including among magnets. For example, the standard description of both the critical region and the phase transition is significantly violated in the metal oxide compound NaV_2O_5, whose magnetic structure is a spin ladder with a $1/4$ filling [16]. In particular, the analysis of data on the dielectric constant, heat capacity, magnetic losses, and ultrasound propagation speed in this material has shown that various physical quantities exhibit identical temperature dependences above and below the phase transition point, regardless of the chosen method of description (power-law or logarithmic divergences). In addition, deviations from the standard theory of phase transitions discovered in [16] include asymmetry of the critical behavior and the presence of an anomalous baseline.

The purpose of this paper is not to extend the list of 'exceptions to the rules.' Instead, we try to demonstrate the existence of a wide range of interesting magnetic phenomena that have not yet been included in the generally accepted taxonomy of magnetic transitions, and for which the term 'spin-fluctuation transition' (SFT) was proposed in [17]. By definition, the characteristics of spin fluctuations changes sharply under an SFT, and this change is not necessarily associated with the emergence or alteration of long-range magnetic order in the system. For an experimenter, SFTs are no less real than ordinary magnetic phase transitions and are therefore often confused with them. From a theoretical standpoint, SFTs have not been sufficiently studied, and it is not yet clear whether a consistent description of SFTs would require fundamental changes to be made in the prevailing paradigm. Because phase transitions in liquids and liquid crystals can be considered the closest analogues of SFTs, at least some SFTs may well be incorporated into the existing theoretical scheme. However, there are SFTs for which the known options of theoretical description are apparently insufficient, and the study of SFTs can therefore stimulate the development of our ideas about phase transitions.

We note that over the past decades a number of reviews have been published on topical problems in the physics of magnetic phenomena (see, e.g., [18, 19]). However, even if these publications touch upon the spin-fluctuation problem, it is not the main subject of the analysis. In addition, it is known that fluctuations cause the appearance of a number of features in lower-dimension systems, for example, in two-dimensional systems with the Berezinskii–Kosterlitz–Thouless transition [20] or in quasi-one-dimensional spin chains [21]. In this review, we consider three-dimensional systems with SFTs, and the problem setting and results of possible SFTs in lower-dimensional systems will be the subject of subsequent publications.

In considering spin fluctuation phenomena, we speak about fluctuations of the vector field of the magnetization of the system, and it must therefore be taken into account that, unlike fluctuations in scalar quantities (pressure, temperature, density, particle number, etc.), fluctuations in vector quantities can differ not only in size but also in direction. Two types of effects can then arise: a sharp change in the amplitude of fluctuations and a change in the anisotropy of fluctuations, which consists, for example, in the transition from isotropic to anisotropic fluctuations. As we show below, both these possibilities not only follow from theoretical models but also are observed experimentally.

This paper is organized as follows. We begin with the history of the development of theoretical ideas about SFTs and consider methods for studying them. After this, examples of SFTs known from experiment are discussed. In conclusion, we return to the ungratifying task mentioned at the beginning of this section and consider the possible systematics of SFTs.

2. Theoretical models

2.1 Spin fluctuations and spin polarons

Surprisingly, SFTs appeared in the theory of magnetic phenomena quite a long time ago. A typical SFT arises in Moriya's theory of itinerant magnetism [22]. The initial goal of this theory was to explain the paradoxical properties of some magnetic metals, for which data on the temperature dependence of magnetic susceptibility in the paramagnetic phase yield an effective magnetic moment μ^* of the order of the Bohr magneton per magnetic ion, $\mu^* \sim \mu_B$, but the saturation magnetic moment in the ferromagnetic phase M_0 is much less than μ_B (for such materials, the term 'weak itinerant ferromagnets' is used in the literature). The explanation of the paradox, according to [22], is that the spin density is not localized on magnetic ions but is distributed over the unit cell of the crystal. The central quantity in Moriya's theory is the amplitude of spin fluctuations $S_L(T)$, which is used to describe the temperature dependence of the Curie–Weiss-type susceptibility with some effective parameters not directly related to the magnitude and concentration of the elementary magnetic moments [22]. At the same time, in the framework of this approach, we have $S_L^2(T_C) = (3/5)M_0^2$ [22], and hence just the saturation magnetic moment has a direct physical meaning.

According to [22], in a system with ferromagnetic correlations, the amplitude of spin fluctuations is given by

$$\left[S_L(T)\right]^2 = \left[S_L(T_{sf})\right]^2 \frac{T}{T_{sf}} \quad \text{at} \quad T \geqslant T_{sf}\,, \tag{1}$$

$$\left[S_L(T)\right]^2 = \left[S_L(T_{sf})\right]^2 \left[1 + \frac{2\left(1 - (T/T_{sf})^{4/3}\right)}{3}\right] \quad \text{at} \quad T < T_{sf}\,. \tag{2}$$

It is easy to see that $S_L(T)$ given by Eqns (1) and (2) has a minimum at a characteristic temperature T_{sf} corresponding to a sharp change in the amplitude of spin fluctuations. In [22], T_{sf} is interpreted as the temperature of the transition from the paramagnetic phase to the ferromagnetic phase (Curie temperature T_C), and hence the paramagnetic–ferromagnetic phase transition is a version of an SFT.

We note that neither Moriya's theory nor its subsequent modifications [23, 24] provide an answer about the nature of another paradoxical property of 'weak itinerant magnets,' associated with the field dependence of the magnetization $M(B)$. For example, for manganese monosilicide (MnSi), which is considered a good example of the successful application of Moriya's theory [22], the effective magnetic moment μ_{eff}, which determines the slope $\partial M/\partial B$ in a weak magnetic field, is $\sim (5-6)\mu_B$, which is different from $\mu^* \sim (1.2-1.3)\mu_B$. The magnetic saturation moment is then of the order of $M_0 \sim 0.3\mu_B$/Mn [25]. In the case of substitutional solid solutions $Fe_xCo_{1-x}Si$, which are also classified as 'weak itinerant magnets,' the anomaly of the field dependence is even more pronounced, and the effective magnetic moment can reach values $\mu_{eff} \sim 13\mu_B$ [26], while the parameter M_0 lies in the range of $(0.05-0.2)\mu_B$/Co [27]. The lack of explanation for the anomalously large values of μ_{eff} is probably a consequence of the conceptual shortcoming inherent in models based on the dominant role of spin fluctuations. A characteristic feature of such theories is the effect of suppression of spin fluctuations by a magnetic field [22–24], and the magnetic field therefore 'destroys' the basis for considering magnetic properties in a finite magnetic field within this approach. These difficulties of the theory of itinerant magnetism can be overcome in a consistent manner in the framework of the spin-polaron model [17, 25, 28, 29], which yields a complete description for the entire set of static and dynamical magnetic properties of materials such as MnSi and $Mn_{1-x}Fe_xSi$, including features of their magnetic phase diagrams.

In general, the concept of spin (magnetic) polarons is used to describe a wide range of phenomena in strongly correlated electron systems. Various types of self-localized states, as well as ferron- and fluctuon-type states, can then be considered [30]. In cases involving changes in the electron dynamics and renormalization of the effective mass, a spin polaron is understood as an electron moving through a crystal and carrying spin polarization due to the interaction with localized magnetic moments (LMMs). This approach has been developed in recent years for two-dimensional systems and has been used to describe superconducting cuprates [31]. The spin polarons considered in this paper are close to the bound states that arise at low temperatures in the Kondo model [32], when the interaction between conduction electrons and LMMs leads to LMM screening. We note that the formation of magnetic polarons also follows from some models of concentrated Kondo systems (to be discussed in more detail in Section 4.3 below when describing the Yu–Min scenario).

The spin-polaron model [17, 25, 28, 29] was originally proposed to explain electron paramagnetic resonance [28], and then demonstrated its effectiveness in a joint description of electrical conductivity and magnetic properties, as well as in constructing magnetic phase diagrams [25]. In addition, spin polarons naturally explain the striking similarity of the temperature dependence of the electrical conductivity of MnSi in the vicinity of the ferromagnetic transition (including the 'fine structure' of the resistivity derivative with respect to temperature and its evolution under high pressure [25, 33]) with experimental data for a classical compound with spin polarons, EuB_6 [34, 35].

Studies of the dynamical magnetic properties of MnSi clearly show that the magnetic subsystem of manganese monosilicide consists of LMMs [17, 25, 28]. This result is consistent with those of LDA calculations, according to which the MnSi spin density is localized on manganese ions and the magnitude of such LMMs is $\mu_{Mn} \approx 1.2\mu_B$ [36]. In such

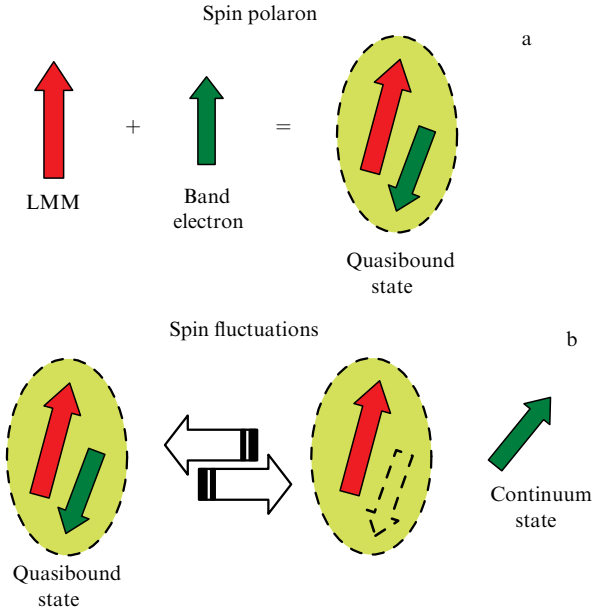

Figure 1. (a) Formation of a spin polaron (a quasibound state of band electrons and LMMs in a crystal). (b) Spin fluctuations caused by the transition of an electron from a quasibound state to the band continuum.

a situation, the small value of the saturation magnetic moment is associated with the screening of manganese LMMs by band electrons in spin-polaron states. In essence, such states are quasibound states of band electrons and LMMs, in which the LMMs and electron magnetic moments are oriented antiparallel (Fig. 1). Such a structure can be considered a nanosize ferrimagnetic cluster, and it can be shown that, for a certain configuration of spins inside the cluster, its magnetization rapidly saturates as the magnetic field increases, which corresponds to the 'giant' magnitudes $\mu_{\text{eff}} \gg \mu^*, \mu_{\text{B}}$ [29]. In the spin-polaron model, the expression for the Curie constant involves the concentration and the corresponding magnetic moment of magnetic ions [29].

The spin-polaron model not only explains the majority of magnetic properties but also naturally gives rise to spin fluctuations associated with electron transitions between quasilocalized states in the vicinity of the LMMs and band states (see Fig. 1). Because spin fluctuations are then of an electron nature, it can be assumed that, to describe them or at least qualitatively assess spin fluctuation effects, model expressions (1) and (2) deduced from Moriya's theory can be used. The temperature T_{sf} should then be interpreted as the temperature of the ordering of spin fluctuations in the spin-polaron state, not necessarily coincident with the temperature of the transition to the magnetically ordered phase [37].

2.2 Brazovskii's theory and helical magnets

In the theory of phase transitions, a situation is known when strong fluctuations change the transition order: instead of a second-order transition, a first-order transition occurs at a critical temperature T_{c} that is lower than the transition temperature T_{MF} in the mean-field approximation. At the phase transition point, the divergence of the correlation length R_{c} disappears. A general theoretical description of such a specific phase transition was given by Brazovskii [38]. We are interested in generalizing the theory in [38] to the case of helical magnets (including the already mentioned manganese monosilicide, MnSi), which typically have an extended fluctuation region in the vicinity of the phase transition [39].

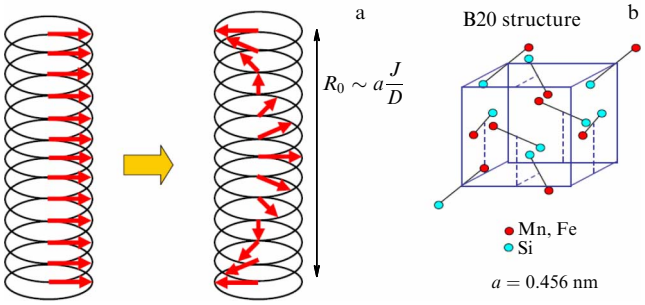

Figure 2. (a) Magnetic helix arising as a result of the combined influence of ferromagnetic exchange and the Dzyaloshinskii–Moriya interaction. (b) Unit cell of the B20 structure into which MnSi and substitutional solid solutions $Mn_{1-x}Fe_xSi$ crystallize.

The magnetic structure of a helical magnet with Heisenberg LMMs can be obtained using the Hamiltonian

$$\hat{H} = \hat{H}_{\text{ex}} + \hat{H}_{\text{DM}} = -J\sum_{i\neq j}\mathbf{S}_i\mathbf{S}_j + \mathbf{D}\sum_{i\neq j}\mathbf{S}_i \times \mathbf{S}_j\,, \qquad (3)$$

where $\hat{H}_{\text{ex}}$ describes the ferromagnetic exchange with energy J, and $\hat{H}_{\text{DM}}$ defines the Dzyaloshinskii–Moriya interaction with the Dzyaloshinskii vector $\mathbf{D}$. If the Dzyaloshinskii energy is zero ($D = 0$), ferromagnetic ordering arises in the magnet, and a nonzero vector $\mathbf{D}$ twists the magnetic structure into a spiral. In known experimental objects, the condition $J \gg D$ is satisfied and an incommensurate magnetic structure with pitch R_0 of the order of $R_0 \sim aJ/D \gg a$ emerges, where a is the lattice constant (Fig. 2a).

The Dzyaloshinskii–Moriya interaction must be allowed by the symmetry of the crystal and typically appears in crystals without an inversion center. Such structures include the group B20, in which MnSi and substitutional solid solutions $Mn_{1-x}Fe_xSi$ crystallize (Fig. 2b). For MnSi, $R_0 = 180$ Å [39], and the helical magnetic structure is incommensurate and has a period much greater than the lattice constant. Because the localization radius of spin polarons in MnSi is $\sim a$ [29], the condition $R_0 \gg a$ implies that the Dzyaloshinskii–Moriya interaction can be neglected when describing spin-polaron states, and LMMs are the reduced magnetic moments of spin polarons [29]. Therefore, Hamiltonian (3) is then an approximation, because it does not include the interaction of band electrons and LMMs and the formation of quasibound states.

In a generalization of Brazovskii's theory in [39], the possibility of SFTs is not considered, but several spin fluctuation regimes arise, smoothly transforming one into another. The crossover region between different types of spin fluctuations is determined from the condition $R_{\text{c}} \sim R_i$, where R_i is the spatial scale associated with a certain type of interaction in the system and R_{c} is the correlation length that determines the magnitude of spin fluctuations [39]. The role of R_i in the theory in [39] is played by the length $R_{\text{DM}} = f(J/D)$ defined by the Dzyaloshinskii–Moriya interaction and dependent on the ratio of the exchange energy J to the Dzyaloshinskii energy D; the Ginzburg length R_{Gi} [39], which specifies the radius of fluctuations in Landau's theory; and (implicitly) the pitch R_0 of the magnetic spiral in the helical phase. A condition on the hierarchy of scales is then

adopted in the form $R_0 > R_{Gi} > R_{DM}$. As a result, as the correlation length $R_c(T)$ increases with decreasing temperature, fluctuations undergo a transformation: in the range $R_c(T) < R_{DM}$, ferromagnetic fluctuations associated with the main exchange J dominate, whereas, for $R_c(T) > R_{DM}$, the Dzyaloshinskii–Moriya interaction must be taken into account, giving rise to helical (chiral) fluctuations whose size continues to increase to the phase transition point, where the condition $R_c(T_c) = R_0$ must hold. Because $R_{Gi} > R_{DM}$ in the model under consideration, it follows that, for $R_c(T) > R_{DM}$, we can distinguish a range associated with the Ginzburg length, $R_{Gi} < R_c(T) < R_0$, which in [39] is described as a range of strongly interacting chiral fluctuations.

In the version of Brazovskii's theory used in [39], the transition temperature to the helical phase T_c is lower than the transition temperature T_{MF} that a helical magnet would have if the mean field theory were applicable, and T_{MF} and the Ginzburg length R_{Gi} are related as $R_c(T_{MF}) = R_{Gi}$. For a conventional second-order magnetic transition, the inverse correlation length $k = 1/R_c$ has the form [3, 14]

$$k(T) = k_0\left(\frac{T}{T_{MF}} - 1\right)^{\nu}, \tag{4}$$

but, for the Brazovskii transition, the relation obtained in [39] is

$$\left(\frac{k}{k_{Gi}}\right)^2 - \frac{1}{k/k_{Gi}} = \frac{T - T_{MF}}{T_0}, \tag{5}$$

where $k_{Gi} = 1/R_{Gi}$ and T_0 determines the region of thermal smearing of the fluctuation region. It is easy to see that, in the limit of large k (small R_c), when the first term on the left-hand side of (5) dominates, we obtain the inverse radius of fluctuations in the form of expression (4), which is standard in Landau's theory with the critical index $\nu = 1/2$. To achieve full agreement with Landau's theory [2], whence the asymptotic form with $k_0 = k_{Gi}$ follows in the form $k(T) = k_{Gi}(T/T_{MF} - 1)^{1/2}$, we must set $T_0 = T_{MF}$ in Eqn (5).

It follows from expression (5) that the dependence $k(T)$ does not vanish anywhere in the region $T \geqslant T_c$, and therefore the magnitude of fluctuations remains finite even at a temperature equal to the transition temperature $T = T_c$. An additional condition therefore arises in the theory in [39]: $k(T_c) = 1/R_0$. In addition, a change in regime at $R_c \sim R_{DM}$ does not lead to any features in the behavior of the correlation length (Eqn (5)).

We note that Brazovskii considered the application of his general theory [38] to the description of phase transitions in cholesteric liquid crystals [40, 41]. We next see that there is a significant similarity between spin fluctuation phenomena and phase transitions in liquid crystals.

2.3 Spin-fluctuation transition to the spin nematic phase in systems with quadrupole order

The statement about the similarities between liquid crystals and magnets formulated at the end of the preceding subsection looks strange at first glance. Indeed, the simplest liquid crystal phase, nematic, arises as a result of the orientation of rod-shaped molecules that float in the liquid and can rotate through an arbitrary angle. In the transition from the phase of an isotropic liquid, in which the molecules are oriented randomly, to the nematic phase, where a preferred orientation direction (director) appears, the symmetry changes, and hence Landau's theory can be used to describe this transition [12, 13]. The distribution function of molecules with respect to angles is introduced as

$$F(\cos\theta) = \sum_{n=1}^{\infty} a_n P_n(\cos\theta), \tag{6}$$

which is traditionally expanded in a series in Legendre polynomials $P_n(\cos\theta)$, with only even terms remaining in the expansion for nonpolar molecules [13] (here, θ is the angle between the axis of the molecule and the director). In the framework of this approach, it is natural to choose the coefficient a_2 as the order parameter [13]. We also note that, from the mathematical standpoint, the isotropic liquid–nematic phase transition for nonpolar molecules is equivalent to the appearance of quadrupole order [12, 13].

Thus, a liquid crystal is a fundamentally classical system consisting of elements that cannot be considered point-like. In this regard, a natural question arises as to why electrons in a crystal (point-like objects), obeying the rules of quantum mechanics, can behave like rods floating in a liquid and exhibit orientational ordering [42]. Electron nematic effects manifest themselves in experiments in the form of resistivity anisotropy, and the greatest attention of researchers has been attracted to iron-based superconductors, ruthenates, and systems with the quantum Hall effect [42–44]. From a theoretical standpoint, the mechanism underlying the electron nematic effect is not unambiguous. Considered most often are changes in the topology of stripe phases and the Pomeranchuk instability, leading to a deformation of the Fermi surface as a result of ferromagnetic interaction [42].

In the case of magnetic systems, a transition to the spin nematic phase can occur [45]. This transition belongs to SFTs and allows a clear physical interpretation at the qualitative level. For simplicity, we consider a model 3D magnet. In the paramagnetic phase, the average spins at the sites are zero, $\langle S_x\rangle = \langle S_y\rangle = \langle S_z\rangle = 0$, and their fluctuations are the same in all directions, $\langle S_x^2\rangle = \langle S_y^2\rangle = \langle S_z^2\rangle \neq 0$. If an ordinary magnetic transition occurs, then the relations $\langle S_x\rangle = \langle S_z\rangle = 0$ and $\langle S_y\rangle \neq 0$ hold in a magnetically ordered phase (for example, of a ferromagnetic type), describing the situation where all spins are aligned parallel to the y-axis. In the spin nematic phase, the average spin at a site is still zero, and there is no long-range magnetic order, but the fluctuations are no longer equal, and a preferred direction, for example, the x-axis, appears: $\langle S_x^2\rangle \neq \langle S_y^2\rangle = \langle S_z^2\rangle$. From a formal standpoint, this problem reduces to the appearance of a quadrupole order in the system [45], which supports the similarity to classical liquid crystals. Thus, electrons in a crystal do not of course become elongated objects reminiscent of molecules in a liquid crystal; the role of molecules ('rods') is played by anisotropic spin fluctuations. Obviously, systems with quadrupole ordering, for example, cerium hexaboride CeB_6 [45], are to be regarded as candidates for the observation of the spin nematic effect. The corresponding models for this material are described in Section 4.1 below. In addition, the influence of quadrupole effects is also significant for pure cerium; for example, they can be used to describe the $\gamma \rightarrow \alpha$ phase transition [46].

The paramagnetic–spin nematic phase transition is a striking example of an SFT in its modern understanding [17], when the anisotropy of spin fluctuations changes sharply at the transition point, but the magnetic order type does not

change (the spin system remains disordered). Considering the analogy with liquid crystals, we can expect that, in this case, too, Landau's theory can be used to describe the transition. For liquid-crystal phases, the expansion of the free energy Φ in terms of the order parameter Q is typically used in the form [12]

$$\Phi = \Phi_0 + aQ^2 + bQ^3 + cQ^4\,, \tag{7}$$

where Q, for example, can be chosen as $Q = |\langle S_x^2\rangle - \langle S_y^2\rangle|$. However, this approach, despite being obvious, has not yet been applied. In particular, in [45], the authors limited themselves to considering the quantum mechanical aspect of the spin nematic problem. We note that, in the case of magnets, well-known ordering models with the thermodynamic potential expanded in the quadrupole order parameter have previously been repeatedly used only in describing phase diagrams and transitions between various magnetic structures and phases with hidden order.

2.4 Spin-fluctuation transition in the Ising model on random sites

In the foregoing, we discussed spin fluctuations of a dynamical nature in crystals. In [47], the Ising model was considered for magnetic centers randomly located in space and having a concentration n and a Bohr radius a. The interaction energy of centers i and j located at distance r_{ij} was taken into account by using the exponential term with the prefactor

$$J(r_{ij}) = \pm J_0 \left(\frac{r_{ij}}{a}\right)^{5/2} \exp\left(-\frac{2r_{ij}}{a}\right). \tag{8}$$

The sign in (8) determined the type of magnetic interaction in the system, antiferromagnetic or ferromagnetic. In this case, $J(r_{ij})$ is a random variable. The spatial average of the spin $\langle S\rangle$ and spin fluctuations $\langle S^2\rangle$ per center were studied in [47]. It turned out that, for studying spin fluctuation phenomena, the model Ising Hamiltonian with spins $S_{i,j} = \pm 1$ can be conveniently represented as

$$\hat{H} = \frac{1}{2}\sum_{i\neq j} J(r_{ij}) S_i S_j = \frac{1}{2}\sum_i J_i S_i\,, \tag{9}$$

with the exchange energy introduced as $J_i S_i = \sum_{j,j\neq i} J(r_{ij}) S_j$ to define the interaction of a spin S_i with all other spins. Next, the exchange energy distribution functions $w(JS)$ were numerically calculated in the antiferromagnetic and ferromagnetic cases, depending on the dimensionless control parameter na^3. Random centers with antiferromagnetic interaction had been studied in [48], where it was shown that long-range magnetic order does not arise in such a system due to the formation of strongly interacting pairs — antiferromagnetic dimers (the so-called singlet phase [48]). We emphasize that, in contrast to [48], a more precise expression (8) for the exchange integral was used in [47], and an analysis scheme was applied based on the understanding of the importance of the SFT problem, which allowed obtaining fundamentally new results.

Let us consider the behavior of the function $w(JS)$ found in [47] as n increases (Fig. 3). With the description method discussed above, the plot is divided into two symmetric halves, corresponding to the spins $S = +1$ and $S = -1$, and the chemical potential is located at the point $JS = 0$ [47]. The change in the distribution function with a change in

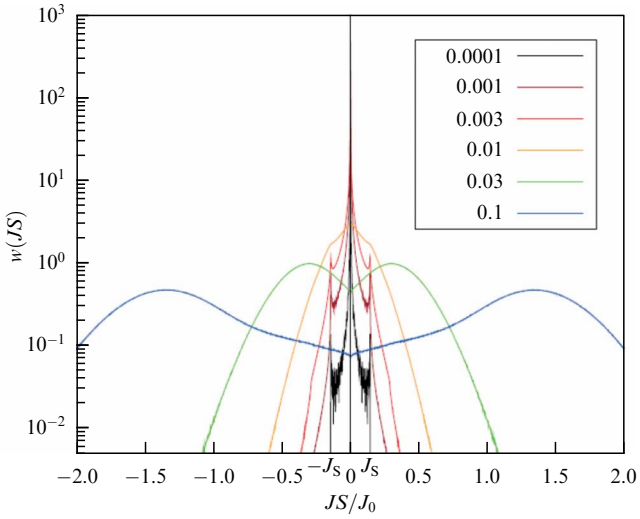

Figure 3. Exchange energy distribution function in the Ising model on random sites in the ferromagnetic case. Inset shows the values of parameter na^3. Narrow peak characteristic of the dimer phase disappears at concentration $na^3 \sim 0.01$. When the concentration of magnetic centers exceeds this value, the system passes into the Gaussian phase. (From [47].)

concentration is qualitatively the same in the antiferromagnetic and ferromagnetic cases, and we therefore consider the data for a system with ferromagnetic interaction (see Fig. 3). At small n, $w(JS)$ has two pronounced peaks due to the predominant influence of pairs of strongly interacting centers on the magnetic properties. For antiferromagnetic interaction, these peaks correspond to the singlet phase (antiferromagnetic dimers with zero total spin) [48], and, for ferromagnetic interaction, to ferromagnetic dimers (in [47], the term 'singlet phase' is somewhat misleadingly used in all cases of dimer formation). As the concentration of centers increases, the distribution function $w(JS)$ transforms into broad singularities (a 'Gaussian phase' in the terminology in [47]). The transition from the dimer phase to the Gaussian phase is then abrupt [47] and occurs at $na^3 \sim 0.01$ (see Fig. 3). However, the most conspicuous physical phenomenon that occurs in this model is the SFT in the Gaussian phase.

The evolution of spin fluctuations in the case of ferromagnetic interaction as a function of the ratio of the Bohr radius to the average distance between centers $r = n^{-1/3}$ is shown in Fig. 4 in accordance with the data in [47]. We can see that the system switches between states with $\langle S^2\rangle \sim 5$ and $\langle S^2\rangle \sim 6000$ in the range $0.4 < a/r < 0.6$, and $a/r \approx 0.5$ can be taken as the transition point (Fig. 4).

We emphasize that magnetic order does not arise in the model under consideration, and the average spin at a center is zero in the entire range of parameters studied in [47]. Thus, in the Ising model, the SFT occurs at random centers with ferromagnetic interaction where the amplitude of spin fluctuations changes significantly [47]. Interestingly, in the model with antiferromagnetic interaction, the change in $\langle S^2\rangle$ with varying a/r is not so pronounced [47], but in that case an SFT point can be identified at which the functional dependence $\langle S^2\rangle = f(a/r)$ changes. We also note that the most significant transformation of the mean square of spin fluctuations occurs in the vicinity of concentrations characteristic of the metal–insulator transition in doped semiconductors.

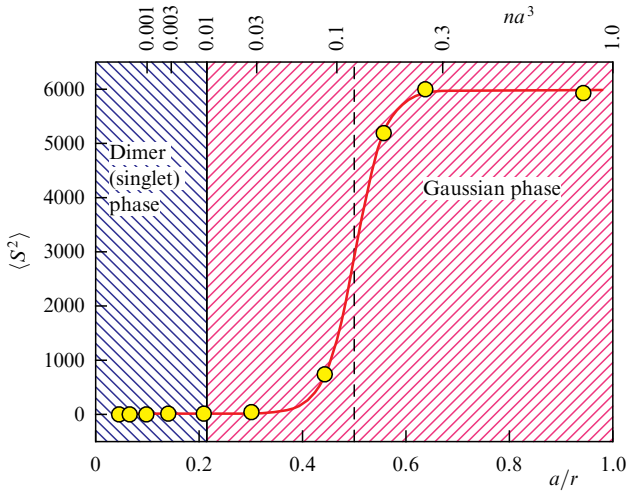

Figure 4. SFT in the Ising model on random sites in the ferromagnetic case. Average value of the spin square S^2 when the inverse reduced distance a/r between magnetic centers switches between two states with $\langle S^2 \rangle \sim 5$ and $\langle S^2 \rangle \sim 6000$ at $a/r \sim 0.5$. Magnetic order does not arise in this case. (Based on [47].)

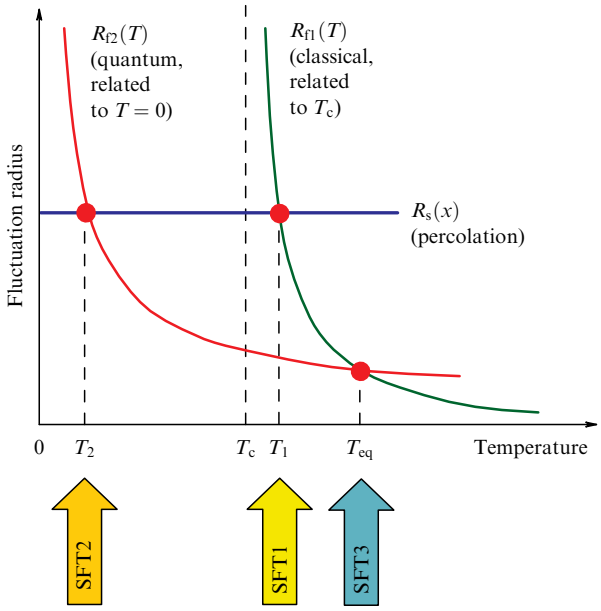

Figure 5. SFTs in the model of a magnetic phase diagram with the coexistence of classical and quantum fluctuations [49]. SFT1 and SFT2 transitions occur when the radius of one fluctuation or another equalizes with the correlation radius of an infinite cluster that depends on the disorder in the system. Another SFT (SFT3) is determined by the coincidence of the radii of quantum and classical fluctuations.

2.5 Spin-fluctuation transitions on magnetic phase diagrams

The idea to determine the boundaries of spin fluctuation phases on a magnetic phase diagram based on a comparison of different spatial scales in the presence of disorder in a crystal was proposed in [49]. The role of characteristic lengths was played by the correlation length of classical fluctuations in the spirit of Landau's theory, R_{f1}, given by an expression similar to (4) with $a_1 = k_0^{-1}$, $T_c = T_{MF}$, and $\nu_1 = \nu$, as well as by the correlation length for quantum fluctuations R_{f2} [50]:

$$R_{f1} = \frac{a_1}{(T/T_c - 1)^{\nu_1}}, \quad R_{f2} = a_2 \frac{T_0}{T}. \tag{10}$$

The parameters a_2 and T_0 in the expression for R_{f2} define the respective spatial and energy scales for quantum fluctuations. Next, the control parameter x that defines the disorder in the system is introduced, with the associated percolation-type correlation radius given by [51]

$$R_s = R_c(x) = \frac{l}{(1 - x/x_c)^{\nu}}, \tag{11}$$

where x_c is the percolation threshold, $\nu \sim 0.9$ is the critical exponent in the three-dimensional system, and l is the minimum length, of the order of the size of the unit cell, corresponding to the ordered case ($x = 0$) [49].

According to [49], different SFTs arise when characteristic lengths (10) and (11) become equal (Fig. 5). The conditions $R_{f1} = R_s$ and $R_{f2} = R_s$ give rise to SFT1 and SFT2 transitions at the temperatures

$$T_1(x) = T_c(x)\left[1 + \frac{\Delta T(0)}{T_c(0)}\left(1 - \frac{x}{x_c}\right)^{\nu/\nu_1}\right],$$
$$T_2(x) = T_2(0)\left(1 - \frac{x}{x_c}\right)^{\nu}. \tag{12}$$

In Eqns (12), $\Delta T(0) = T_1(0) - T_c(0) = (a_1/l)^{1/\nu_1} T_c(0)$ and $T_2(0) = (a_2/l)T_0$. The condition $R_{f1} = R_{f2}$ corresponds to SFT3 at the temperature $T_{eq}(x)$, separating the regions dominated by classical and quantum fluctuations (see Fig. 5). If $\nu_1 = 1/2$, then $T_{eq}(x)$ can be found from the equation

$$A = \frac{z^2}{z - 1}, \tag{13}$$

where $z = T_{eq}(x)/T_c(x)$ and $A = T_2^2(0)/\Delta T(0) T_c(x)$. Let the dependence $T_c(x)$ of the temperature of the transition to a phase with long-range magnetic order on the control parameter be known from experiment and the SFT1 temperature $T_1(0)$ in the absence of disorder, at $x = 0$, also be known. Two parameters then suffice to specify the $T-x$ magnetic phase diagram: the percolation threshold x_c and the energy scale associated with quantum fluctuations $T_2(0)$ [49].

The model in [49] partly resembles the approach used in [38, 39], although the change in the fluctuation regime for different relations between spatial scales is understood there not as a crossover but as an SFT with a well-defined transition temperature. Another feature of the description of the $T-x$ diagram proposed in [49] is the coexistence of two types of fluctuations, quantum and classical, for any x, not only at the quantum critical point. There is currently no rigorous theoretical justification for such a hypothesis, although, for specific magnetic systems, arguments can be made in favor of the possibility of the coexistence of different types of fluctuations. It is therefore of interest to compare the results in [49] with experiment, first of all selecting those that cannot be obtained in the framework of classical theories or their generalizations [38, 39]. In particular, the model in [49] predicts an SFT3 transition at $T_{eq}(x)$ to be observed in the paramagnetic phase for $T_{eq} > T_1, T_2$ (see Fig. 5). Another interesting consequence is the possibility of an SFT inside the magnetically ordered phase when the condition $T_c(x) > T_2(x)$ is satisfied [25]. As we show in subsequent sections, these nontrivial consequences of the model in [49]

are confirmed experimentally. In addition, the considered approach allows quantitatively describing the $T-x$ magnetic phase diagram of substitutional solid solutions $Mn_{1-x}Fe_xSi$ [49]. In this case, the control parameter x (disorder in the system) can be related to the concentration of iron in the solid solution.

It is worth noting how the SFT develops when the magnitude of fluctuations reaches the correlation radius associated with disorder. In [49], it was assumed that R_s bounds the increase in the magnitude of fluctuations as temperature decreases because, having 'captured' structural inhomogeneities or defects, fluctuations freeze and their radius no longer increases, remaining constant [49]. However, this behavior contradicts experimental data on the temperature dependences of the correlation length [39, 52] in spin-fluctuation phases. Obviously, in a system with structural disorder, a spherically symmetric fluctuation can exist only in the range $R_f < R_s$, and in the range $R_f > R_s$ the fluctuations interact with structural defects and apparently cannot grow equally in all directions. In that situation, an anisotropic fluctuation regime can arise, for example, as a result of the presence of small anisotropic terms in the spin Hamiltonian, the influence of an external field, or spontaneous symmetry breaking, when one fluctuation randomly extended along some direction would determine the orientation of fluctuations at neighboring spatial points. We can therefore expect the resulting spin-fluctuation phase at $R_f > R_s$ to be characterized by anisotropic spin fluctuations characteristic of the spin nematic phase. Another option for the occurrence of the spin nematic effect is the possibility for correlations setting in to correspond to an initially anisotropic spin fluctuation in a magnetic system. This case can also be realized in helical magnets.

3. Experimental methods for studying spin-fluctuation transitions

It is obvious that studying SFTs requires the use of methods that are sensitive to spin fluctuations. This trivial statement is not always easy to implement in practice, because the use of popular physical characteristics in the field of magnetic phenomena such as magnetization, magnetic susceptibility, and magnetoresistance requires a priori information that these quantities depend on the spin-fluctuation regime of the sample under study. But this can only be judged on the basis of certain theoretical models, among which 'suitable' ones should be selected depending on the description preferred by the researcher. This methodology is unpromising for the demonstrative identification of the group of magnetic phenomena under consideration. Nevertheless, experimental methods for studying spin fluctuations exist, and using them allows obtaining reliable data on SFTs.

3.1 Neutron scattering

We consider the use of small-angle neutron scattering (SANS) to solve the problem posed by discussing example of helical magnets — substitutional solid solutions $Mn_{1-x}Fe_xSi$ [53]. SANS polarization experiments demonstrate a change in the scattering pattern with temperature (Fig. 6). In the paramagnetic phase $T > T_1$ (region *1*), scattering is isotropic. In the range $T < T_1$ (regions *2* and *3*), a characteristic crescent-shaped structure appears, which becomes more pronounced as the temperature decreases. Interestingly, this scattering pattern is identical to the X-ray scattering data for the

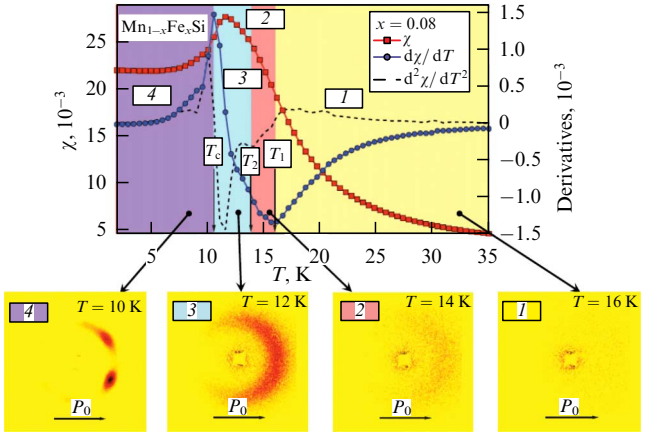

Figure 6. Relation between evolution of small-angle scattering map of polarized neutrons and temperature dependence of magnetic susceptibility in $Mn_{1-x}Fe_xSi$ substitutional solid solutions in the example of a single crystal with $x = 0.08$. *1* — paramagnetic phase; *2*, *3* — phase with anisotropic spin fluctuations, *4* — magnetically ordered (helical) phase. (From [53].)

nematic phase of liquid crystals [13]. We therefore relate this behavior to the regime of anisotropic spin fluctuations. A further decrease in temperature leads to the transformation of the crescent into Bragg peaks, indicating the formation of a helical magnetic phase with long-range magnetic order at $T \leqslant T_c$ (region *4*). According to [39, 53], the temperature T_1 is determined by the Dzyaloshinskii–Moriya interaction, $T_1 \sim D/k_B$, and isotropic ferromagnetic fluctuations in the system transform into helical ones at this temperature. Helical fluctuations are obviously anisotropic, and parts of spin spirals dynamically appearing in the bulk of the sample play the role of rod-shaped molecules in liquid crystals, which explains the similarity of scattering patterns [13, 53]. Thus, at $T = T_1$, $Mn_{1-x}Fe_xSi$ undergoes an SFT into the spin nematic phase (see Section 2.3).

It is noteworthy that, at characteristic temperatures T_1 and T_c, not only does the neutron scattering pattern change but also features appear in the temperature dependence of the magnetic susceptibility derivative $\partial\chi/\partial T$ (see Fig. 6). It was found in [53] that the temperature T_1 corresponds to a minimum, and the temperature T_c, to a maximum of $\partial\chi/\partial T$. This result has practical significance for the study of magnetic transitions and SFTs in $Mn_{1-x}Fe_xSi$. Once the relation between the properties of a physical quantity (in this case, magnetic susceptibility) and structural data that provides information about spin fluctuations is established, this 'secondary' characteristic can be used to identify SFTs. Measuring $\chi(T)$ is a simpler and less expensive task than conducting neutron experiments.

It is assumed in [53] that, in the range $T < T_1$, another characteristic temperature T_2 can be identified that separates the regions *2* and *3* in Fig. 6. The boundary between the regions, as proposed in [53], is associated with the singularity of the second derivative $\partial^2\chi/\partial T^2$. Helical fluctuations in the range $T_c < T < T_2$ are then more pronounced than in the range $T_2 < T < T_1$ while maintaining the qualitative neutron scattering pattern. A more transparent physical reason can also be adduced to identify this boundary within the range $T < T_1$. For this, we can use the data on the inverse lifetime of spin fluctuations Γ, which was found in [53] using neutron spin echo data (Fig. 7). It is easy to see that, at $T = T_2$, the

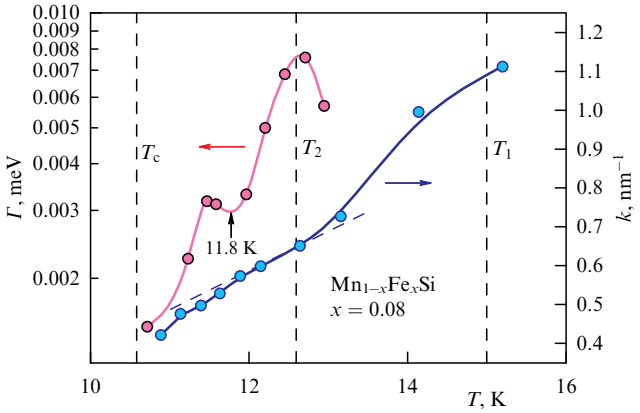

Figure 7. Temperature dependences of inverse correlation length k and spin fluctuation frequency Γ (in energy units) for an $Mn_{1-x}Fe_xSi$ sample with $x = 0.08$. (From [53].)

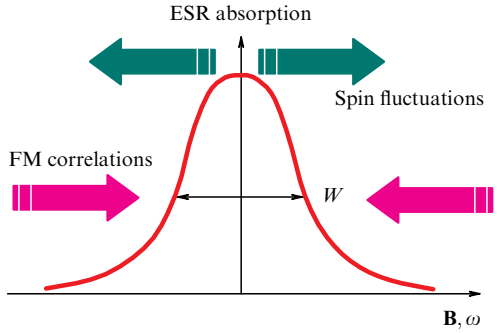

Figure 8. Influence of ferromagnetic correlations and spin fluctuations on the EPR linewidth in strongly correlated metals. Spin fluctuations broaden the line, and ferromagnetic (FM) correlations reduce its width. (Based on [17].)

temperature dependence $\Gamma(T)$ has a maximum, indicating a change in the spin-fluctuation dynamics under some SFT. We note that, in the sample with $x = 0.08$, the $\Gamma(T)$ curve has yet another feature at $T \sim 11.8$ K corresponding to a minimum of the second derivative of the magnetic susceptibility with respect to temperature (see Fig. 6). Thus, the study of relaxation characteristics indicates the existence of another SFT in $Mn_{1-x}Fe_xSi$, associated with a change in the dynamical characteristics of spin fluctuations.

In neutron scattering studies [39, 53], it is often stated that SANS data allow determining the correlation length, i.e., the radius of fluctuations. These data are typically given in the form of the dependence $1/R_c = k(T)$. Experiment actually allows determining the effective size of the coherent scattering region, which is identified with the correlation length of spin fluctuations. As far as we are aware, anisotropic characteristics of spin fluctuations from neutron scattering data have not yet been determined. An example of the experimental dependence $k(T)$ is shown in Fig. 7. It can be seen that, under the SFT in the range $T < T_1$, the slope of the $k(T)$ curve changes, and therefore the derivative $\partial k/\partial T$ acquires SFT-related features. Thus, SFTs can manifest themselves in both the dynamical and spatial characteristics of spin fluctuations, and a sharp change in the fluctuation radius can be used to detect an SFT.

3.2 Electron paramagnetic resonance

The problem of the influence of spin fluctuations on the characteristics of electron paramagnetic resonance (EPR) in various systems with strong electron correlations was recently addressed in review [17]. It follows from the analysis performed that is the EPR linewidth W the most sensitive to the effect of spin fluctuations [17]. The currently known theoretical results for systems with strong electron correlations amount to the fact that spin fluctuations broaden the absorption line, while ferromagnetic correlations 'strive' to make the resonance narrower [54–56] (Fig. 8). The narrowing of the EPR line is regarded as a generalization of the classical Korringa spin relaxation mechanism [56], for which $W \sim 1/\chi(T)$ because the magnetic susceptibility increases in the ferromagnetic case. We note that, in addition to spin fluctuations, antiferromagnetic correlations can also lead to EPR line broadening, leading to a decrease in $\chi(T)$.

Thus, a change in the EPR linewidth as a result of an SFT can occur in the background of a temperature dependence caused by magnetic interactions in the system under study. This may complicate the identification of the relevant spin-fluctuation contribution. However, it turns out that SFTs occur in the $W(T)$ temperature dependence in the form of sharp features, similarly to the $\Gamma(T)$ data (see Fig. 7).

In addition, to study an SFT into the spin nematic phase, it may be useful to study the angular dependence of the linewidth. Indeed, if the anisotropy χ is small or known, then in the spin-nematic phase we can expect a stronger angular dependence of W or its modification compared with the magnetic susceptibility anisotropy. As in the case of neutron experiments, the EPR data used to find the SFT can be associated with some 'secondary' physical quantity, changes in which can be used to identify the SFT. This approach turned out to be effective for studying the SFT in CeB_6, to be discussed in Section 4.

A problem may be encountered in determining the type of fluctuations, i.e., deciding which fluctuations, quantum or classical, lead to the observed transition. For a concentrated Kondo system, an analysis in the framework of the Fermi liquid theory, which includes both the strong interaction between band electrons and LMMs and the ferromagnetic correlations, was performed in [54–56]. It was shown that the change in the g-factor is negligible, and the leading effects are to be seen in the linewidth that depends on the temperature in accordance with the law $W = W_0(1 + AT^2)$.

A possible modification of the spin dynamics in the framework of the semiclassical Landau–Lifshitz equation with quantum fluctuations of the magnetic moment taken into account was considered in [57]. In the case of classical magnetization fluctuations, only the linewidth changes, and the resonance frequency (the g-factor) does not shift. Quantum fluctuations are characterized by a correlation between fluctuations in the spin precession frequency and magnetization fluctuations in the direction parallel to the external constant magnetic field [57]. This implies that the shift of the g-factor and the spin fluctuation contribution to the EPR linewidth are related to each other [57]:

$$\frac{\Delta g_{QF}}{g} \approx -\frac{v^2}{\omega^2}\, a_0\,, \tag{14}$$

$$\frac{\Delta W_{QF}}{W_0} \approx a_0\,. \tag{15}$$

Here, ω and ν are the respective frequencies of microwave radiation and spin relaxation; a_0 describes the effect of quantum fluctuations and can be estimated as $a_0 \sim 2\Delta M_z^2/\mu_B M_0$, where ΔM_z and M_0 are the amplitude of fluctuations and the average magnetic moment per magnetic ion (the external magnetic field is assumed to be directed along the z-axis). The use of Eqns (14) and (15) to identify the type of fluctuation that determines an SFT is discussed below with the example of MnSi. It can also be shown [58] that, in the absence of quantum effects, the fluctuation correction to the linewidth is of the order of $\Delta W \sim \Delta M_x^2, \Delta M_y^2$, where the coordinate axes x and y are directed perpendicular to a constant magnetic field. Thus, if the average spin is zero, $\langle S \rangle = 0$, then, in estimating the spin-fluctuation contribution to the linewidth, we can assume that $\Delta W \sim \langle S^2 \rangle$.

In addition, if we use the classical approach to describe EPR, then the linewidth is inversely proportional to the spin relaxation time, and hence the EPR technique provides combined information about the amplitude of spin fluctuations and their characteristic frequency.

4. Examples of experimental observation of spin-fluctuation transitions

4.1 Spin-fluctuation transitions in the spin nematic phase (cerium hexaboride)

Cerium hexaboride CeB_6 has a simple body-centered cubic (bcc) structure formed by two cubic sublattices made of Ce^{3+} ions and boron octahedra B_6, shown schematically in Fig. 9a. In the physics of strongly correlated electron systems, CeB_6 is usually regarded as an example of a metallic concentrated Kondo system with heavy fermions [59–65]. Despite its simple crystal structure, this compound has a nontrivial magnetic phase diagram due to the interaction of spin and orbital degrees of freedom. In a zero magnetic field, as the temperature decreases, a magnetic transition occurs at $T = T_{AFQ} = 3.2$ K, which precedes the formation of a long-range antiferromagnetic order with a complex structure at $T_N = 2.3$ K. Switching on a magnetic field B leads to an increase in $T_{AFQ}(B)$ and a decrease in $T_N(B)$ [59–65]. This sequence of magnetic transitions in CeB_6 was established using neutron diffraction [59], resonant X-ray scattering [60], heat capacity [61], NMR [62], magnetization [63, 64], and transport measurements [65].

The most popular model concepts in the literature are those relating the physical properties and features of the magnetic phase diagram of CeB_6 to the interaction of quadrupole electric moments of the 4f shells of Ce ions, which result from the splitting of the $^2F_{5/2}$ level by the crystal field [66–72]. Various terms are used to designate the phase existing in the range $T_N < T < T_{AFQ}$: 'antiferroquadrupole phase,' 'orbitally ordered phase,' 'hidden-order phase,' or simply 'phase II.' Such a discrepancy in naming nevertheless corresponds to almost identical model ideas. In most studies, CeB_6 is assumed to have the lowest-energy state Γ_8 with a quadrupole moment. In the paramagnetic phase ($T > T_{AFQ}$), the spins and quadrupole moments of the 4f shells are disordered, but, at $T \leqslant T_{AFQ}$, a three-dimensional lattice appears in which the quadrupole moments $+Q$ and $-Q$ alternate in a checkerboard pattern [59]. The concept of ordering of quadrupole moments is a version of the description of the orbital ordering effect applicable to cerium hexaboride. It is believed that orbital ordering at the boundary $T_{AFQ}(B)$ between the paramagnetic and orbitally ordered phases occurs without changing the lattice constant [60] due to the weak contribution of the 4f electrons to the chemical bond. This highlights a dramatic difference between the orbital effects in CeB_6 and in manganites, where orbital ordering changes both the crystal structure and the magnetic order [73–75].

The magnetic nature of the transition at $T = T_{AFQ}$ manifests itself when an external magnetic field is imposed, giving rise to an additional magnetic moment in the orbitally ordered phase, whose amplitude increases with increasing B; this magnetization component obviously has a 3D checker-

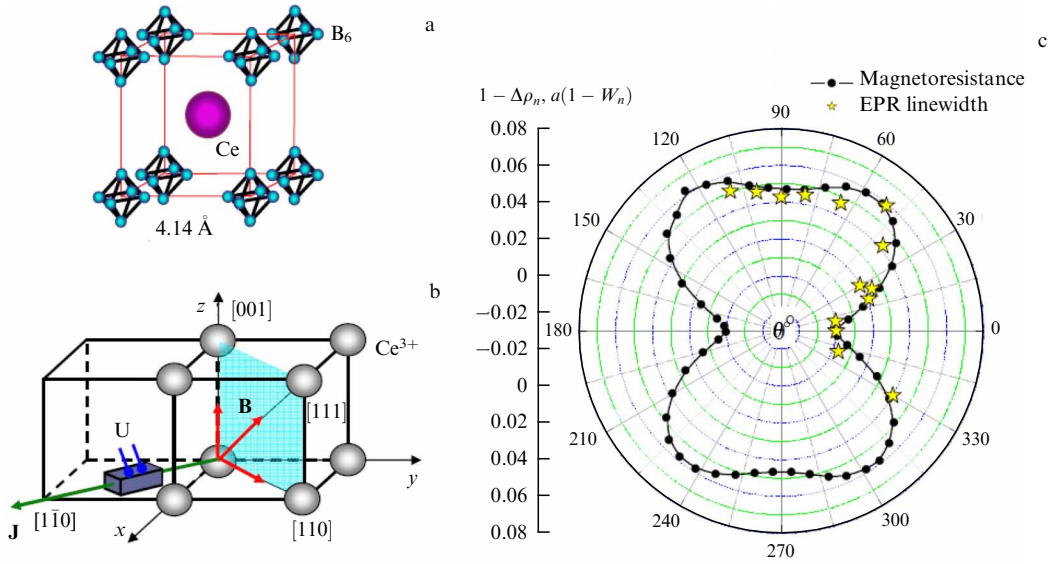

Figure 9. (a) Structure of CeB_6; (b) experimental geometry for studying EPR and magnetoresistance; (c) correlation between angular dependences of the EPR linewidth and magnetoresistance (from [77]). In experiment with rotation, the sample was rotated about the crystallographic direction [1$\bar{1}$0], perpendicular to the external constant magnetic field. In this geometry of the experiment, the external field can be oriented along principal crystallographic directions [001], [111], and [110] (Fig. b). Origin of the angle in Fig. c corresponds to the [001] direction.

board antiferromagnetic structure. Experimentally, this effect is detected in the form of magnetic reflection with the wave vector $\mathbf{k}_0 = [1/2, 1/2, 1/2]$, whose intensity increases with the magnetic field and, in the simplest model, vanishes in a zero magnetic field [59]. This property of the orbitally ordered phase of CeB_6 justifies the term antiferroquadrupole (AFQ) phase, which we use in what follows. The absence at $T = T_{AFQ}$ of the usual type of magnetic order justifies the term 'hidden order' used to denote this type of magnetic transition. We note that the considered model representations constitute a physical description at the *minimum minimorum* level and do not reflect the entire set of phenomena characteristic of the low-temperature magnetic properties of CeB_6. However, the model approach described above is sufficient to understand the SFT problems in this material. We refer those readers who are interested in a more complex picture of the physical properties of the AFQ phase to review [76].

As already noted, in a system with quadrupole order, spin fluctuations must exhibit anisotropy, and a spin nematic phase must form [45]. The anisotropy of spin fluctuations can lead to anisotropy of the angular dependence of the EPR linewidth $W(\theta)$ (see Section 3.2). A low-temperature EPR experiment at a frequency of 60 GHz, with a CeB_6 sample rotated in a magnetic field about the $[1\bar{1}0]$ direction, was performed in [77], where the angular dependence of the line shape in the AFQ phase was obtained and compared with the results of independent measurements along the principal crystallographic directions (Fig. 9b). In [77], the angle $\theta = 0°$ corresponds to direction [001]. It was found that, at $T = 1.8$ K, the EPR linewidth is anisotropic (Fig. 9c), in agreement with theoretical expectations. Moreover, it turned out that the normalized angular dependences of the linewidth $W(\theta)$ and the magnetoresistance $\rho(\theta)$ in the field $B = 2.8$ T, which is close to the magnetic resonance field, are almost identical (Fig. 9c). This result suggests that anisotropic magnetic scattering in CeB_6 occurs on the same spin fluctuations that determine the EPR anisotropy [77]. In addition, we here see the possibility of using a 'secondary' physical quantity, magnetoresistance in this case, to study the SFT. This is fundamentally important for studying the spin nematic phase in this material, because EPR is solely observed in CeB_6 in the AFQ phase, and, as the temperature approaches the phase boundary $T_{AFQ}(B)$, the line broadens so significantly that the magnetic resonance cannot be detected in the paramagnetic phase [17, 76, 77].

The anisotropy of magnetoresistance in cerium hexaboride was studied in detail in [78] in a geometry different from that shown in Fig. 9, with the sample rotated about the [001] axis, along which the measuring current was directed. The magnetic field changed its direction in the plane perpendicular to [001]. First, it was found that, in the range $B \leqslant 3$ T, the angular dependence $\rho(\theta)$ can be represented with high accuracy as the sum of the second and fourth Legendre polynomials [78],

$$\rho(B, T, \theta) = \rho(B, T, 0)\, f(\theta)\,, \qquad (16)$$
$$f(\theta) = 1 + a_2(B, T) P_2(\cos\theta) + a_4(B, T) P_4(\cos\theta)\,.$$

Here, direction [110] is taken as the origin for the angle. We first consider the temperature dependences $a_2(T)$ and $a_4(T)$ in fixed magnetic fields (Fig. 10a, b). It is noteworthy that, as a result of the decrease in temperature below a certain $T_{max}(B)$, finite values of the coefficients a_2 and a_4 appear step-wise,

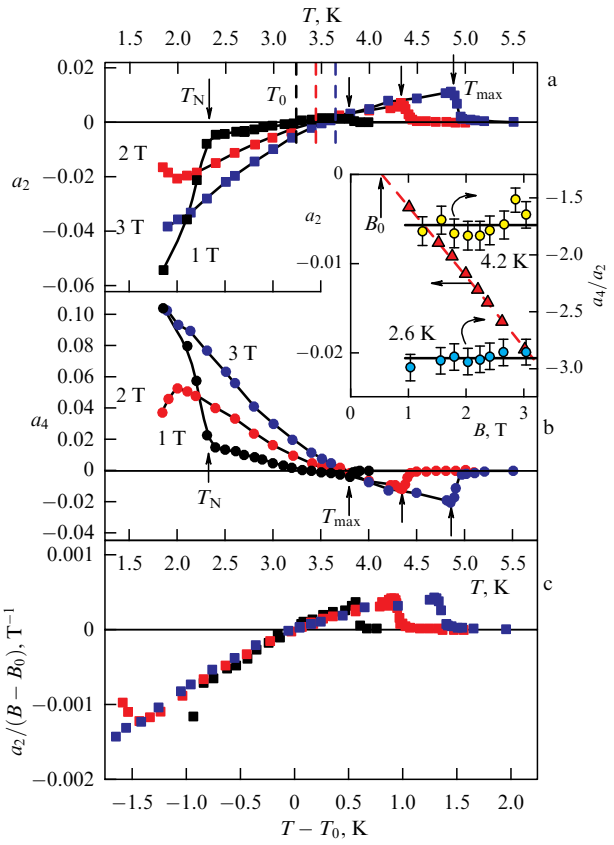

Figure 10. Temperature dependences of the coefficients (a) a_2 and (b) a_4 in Eqn (16) for CeB_6. Inset shows dependence of a_2 on the magnetic field at $T = 2.6$ K and field dependences of the ratio a_4/a_2 at $T = 4.2$ K and $T = 2.6$ K. (c) Scaling of the order parameter. (Based on [78].)

while the range $T > T_{max}(B)$ is characterized by zero values $a_2 = a_4 = 0$. As the temperature decreases in the range $T < T_{max}(B)$, a_2 monotonically decreases and a_4 monotonically increases; at certain temperatures that are close to but not coincident with each other, the sign of these parameters is reversed (Fig. 10a, b). Following [78], we let $T_0(B)$ denote the characteristic temperature at which a_2 changes sign (Fig. 10a). We note that, in addition to the above features, in the field $B = 1$ T, the $a_2(T)$ and $a_4(T)$ curves exhibit a kink associated with the transition to the antiferromagnetic phase (Fig. 10a, b).

The analysis of experimental data carried out in [78] allowed establishing a highly nontrivial fact. We transform Eqn (16) into the form

$$\rho(B, T, \theta) = \rho(B, T, 0)\Big\{1 + a_2(B, T)\big[P_2(\cos\theta) + bP_4(\cos\theta)\big]\Big\}\,, \qquad (17)$$

where $b = a_4/a_2$, and analyze the field dependence of the parameters. In the range $T < T_{max}(B)$, we select two regions in which the temperature is less than or greater than $T \sim 3.5$ K; in each of these regions, the condition $b = \text{const}$ is then satisfied, but the ratios $b = a_4/a_2$ are different (see inset in Fig. 10). The coefficient a_2 depends linearly on the magnetic field, $a_2 \sim B - B_0$, where $B_0 \sim 0.5$ T (inset in Fig. 10). Thus, according to [78], the field and temperature dependence of the anisotropic magnetoresistance of CeB_6 is determined by the coefficient a_2, which can be considered an order parameter for the SFT occurring at $T_{max}(B)$, entirely

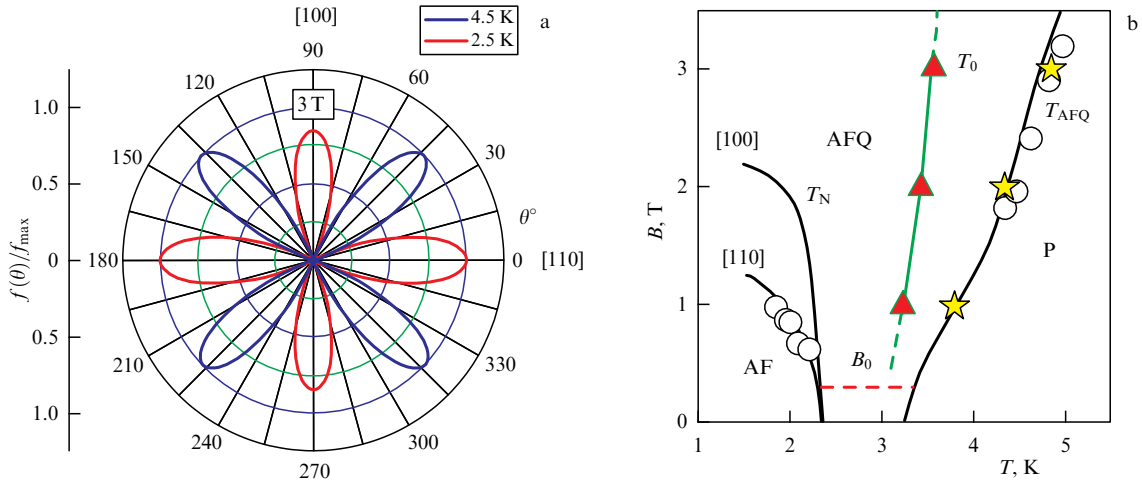

Figure 11. (a) Normalized angular dependences of the magnetoresistance of CeB_6 in a 3 T field at temperatures of 4.5 K and 2.5 K. (b) Magnetic phase diagram of CeB_6 constructed with results of a study of the spin nematic effect taken into account: P — paramagnetic phase, AF — antiferromagnetic phase, AFQ — antiferroquadrupole phase. Solid lines are literature data; white dots are plotted according to the characteristics of microwave absorption. Temperature T_0 (triangles) corresponds to an SFT in the antiferroquadrupole phase. Asterisks show temperature T_{max} at which magnetoresistance anisotropy occurs. Dashed line B_0 shows the expected additional line on the magnetic phase diagram in a weak magnetic field. (Based on [78].)

meets the case of classical liquid crystals [13], and a sharp change in the parameter b reflects a change in the symmetry of spin fluctuations [78]. This effect is illustrated in Fig. 11a, which shows the angular dependences of the normalized function $f(\theta)$ for $T < 3.5$ K and $T > 3.5$ K. We can see that the spatial orientation of spin fluctuations does not remain constant, and the extrema of $f(\theta)$ rotate through 45° at $T \sim 3.5$ K.

In [78], a scaling for the parameter a_2 was also obtained in the form

$$a_2 = (B - B_0)\,\varphi\big(T - T_0(B)\big)\,, \qquad (18)$$

corresponding to the normalization of the amplitude by $B - B_0$ and the shift of the temperature dependence by the sign reversal temperature $T_0(B)$ (Fig. 10c). This analysis indicates the presence of some feature in a weak magnetic field. Interestingly, the corresponding line on the magnetic phase diagram was previously predicted theoretically in [71] and discovered experimentally in [79]. In addition, it turns out that just the characteristic temperature $T_0(B)$ is to be related to the change in the symmetry of spin fluctuations shown in Fig. 11a [78].

We now analyze the results obtained in [78] from the standpoint of theoretical expectations expressed in [45]. For this, we plot the obtained points $T_{max}(B)$ and $T_0(B)$ on the magnetic phase diagram of CeB_6 (Fig. 11b). It can be seen that the temperature $T_{max}(B)$ at which anisotropy occurs is ideally coincident with the boundary between the paramagnetic phase and the AFQ phase. This result is totally consistent with the theory in [45], according to which the spin nematic phase with anisotropic spin fluctuations is the phase with hidden (quadrupole) order. However, as follows from experimental data, a change in the spatial orientation of spin fluctuations at $T_0(B)$ occurs in the range of existence of the AFQ phase, where, according to the currently known structural data, no fundamentally new magnetic order arises, be it conventional or hidden. Thus, it was shown in [78] that CeB_6 undergoes two spin fluctuation transitions, SFT1 and SFT2. The first, SFT1, at the boundary of the AFQ phase, is associated with the appearance of anisotropic spin fluctuations, and the second transition, SFT2, corresponds to a change in the symmetry of spin fluctuations at $T_0(B)$ and is not associated with a change in any magnetic order, i.e., is an SFT *in purissima*. It is obvious that SFT2 in CeB_6 can be considered a spin-fluctuation analogue of the orientation transition in magnetic materials [78].

The special character of SFTs in CeB_6 clearly manifests itself in the unusual scaling of the order parameter (Eqn (18)). Indeed, according to the simplest version of Landau's theory with a single order parameter, we expect scaling with the magnetic transition temperature $T_{max}(B)$, which obviously contradicts experiment (Fig. 10c). At present, it is not clear whether this anomaly can be included in the standard paradigm [2–4], for example, by introducing several interacting order parameters.

We note that SFT1 is accompanied by a heat capacity feature characteristic of first-order phase transitions [61], in full accordance with the liquid-crystal analogy for the transition to the spin nematic phase, because the isotropic liquid–nematic transition refers precisely to this type of phase transition [13]. However, for orientational SFT2, there is no pronounced thermal effect or any heat capacity feature in CeB_6. It cannot be ruled out that this SFT is a crossover; however, the ultimate answer to the question about the nature of this SFT requires the development of theoretical models, which remains a task for future research.

4.2 Toward experimental verification of the SFT in the Ising model on random sites (doped compensated germanium)

To our knowledge, the theoretical results described in Section 2.4 have not yet been subjected to a dedicated experimental test. Nevertheless, the results in [80, 81], whose publication preceded the theoretical prediction of the SFT in the Ising model on random sites [47], are of some interest. In [80, 81], EPR in germanium prepared by neutron doping [82] was studied. This method is based on nuclear reactions that occur when neutrons are captured by isotopes of a semiconducting material, when the sample is exposed to a neutron flux. In the case under consideration, the isotopes ^{70}Ge, ^{74}Ge,

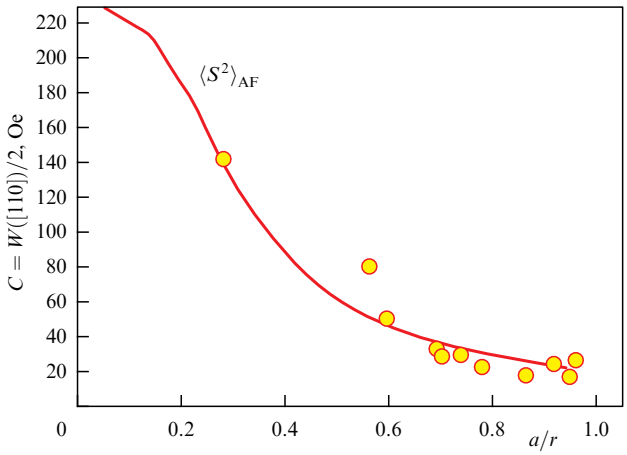

Figure 12. Dependence of EPR line half-width for the [110] crystallographic direction in doped compensated semiconductor Ge:As(Ga) on inverse reduced distance a/r. Dots are experimental data from [80], line is the theoretical calculation of the average value of S^2 in the Ising model in random centers in the case of antiferromagnetic interaction [47].

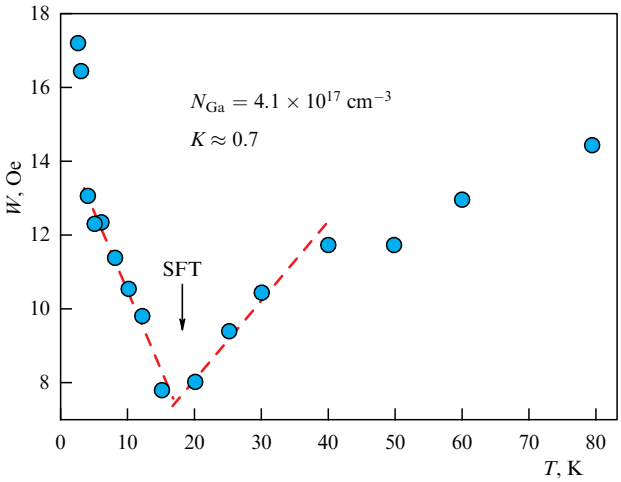

Figure 13. Temperature dependence of the EPR linewidth in a Ge:As(Ga) sample with a gallium content of 4.1×10^{17} cm^{-3} and compensation degree $K = 0.7$ (from [81]). Arrow shows expected spin fluctuation transition at 17 K.

and ^{76}Ge are suitable for producing electrically active impurities that are respectively converted into gallium, arsenic, and selenium as a result of neutron capture. Gallium is an acceptor, and arsenic and selenium are donors. It is important that the neutron doping technique allows effectively controlling the degree of compensation in samples [82].

Ge:As(Ga) crystals initially doped with arsenic and compensated by a gallium impurity introduced into the sample by neutron doping were studied in [80, 81]. In such a system, depending on the doping level and the degree of compensation, both ferromagnetic [83] and antiferromagnetic [80, 81] interactions between impurity centers can emerge. In what follows, we consider data on samples in which the interaction between the spins of donor-localized electrons is antiferromagnetic [80, 81]. In such a system, EPR is observed on neutral donors.

For the study of SFT problems, experimental data on the EPR linewidth are of greatest interest. In [80], the experimental dependence of the parameter $C = W[110]/2$, equal to half the linewidth along the [110] direction of the magnetic field, on the gallium concentration N_{Ga} is given. To compare the data in [80] with the theoretical dependences found in [47], we must first determine the spatial scale a/r. As an estimate, we assume that $a/r \sim a(N_{As} - N_{Ga})^{1/3}$ in compensated samples. Then, apparently, the dependence $C = f(N_{Ga})$ found in [80] could be obtained in samples with slightly different initial arsenic concentration N_{As}, and, in our case, this parameter therefore has the meaning of some effective 'average' concentration of donor centers. We also assume that the leading contribution to the EPR linewidth of Ge:As(Ga) comes from spin fluctuations and $W[110] \sim \langle S^2\rangle$, where the function $\langle S^2\rangle = f(a/r)$ for antiferromagnetic interaction was found in [47]. To compare the theoretical dependence with experimental data, we then have to determine three fitting parameters: a, N_{As}, and the proportionality coefficient between $\langle S^2\rangle$ and W. The result of such an analysis for $N_{As} \approx 4 \times 10^{17}$ cm^{-3} and $a \approx 13$ nm is shown in Fig. 12. It can be seen that the chosen values provide good agreement between the experimental data and the theoretical dependence. We note that, according to [47], the SFT in a system with antiferromagnetic interaction in which dimers disappear and the Gaussian phase is formed occurs at $a/r \sim 0.2$, a value corresponding to the inflection point on the $\langle S^2\rangle = f(a/r)$ curve (see Fig. 12).

Unfortunately, the range of impurity concentrations in the samples studied in [80] is obviously insufficient for testing theoretical predictions in [47]; however, our analysis shows that the study of doped semiconductors by EPR may be promising for detecting the SFT expected in the Ising model on random sites. Interestingly, the estimate $a \approx 13$ nm is somewhat higher than the localization radii for arsenic, a(As) ~ 6 nm, and gallium, a(Ga) ~ 9 nm, impurities in germanium [51]. However, the value we obtained is in good agreement with the characteristic size of antiferromagnetic clusters, ~ 10 nm, which, according to [80, 81], form from neutral donor impurities in Ge:As(Ga). Nevertheless, the question of the effective localization radius involved in the theory in [47] requires additional research.

The temperature dependence of the EPR linewidth may be of significant interest for the detection of SFTs. In Fig. 13, we show the temperature dependence of $W(T)$ for a sample with $N_{Ga} = 4.1 \times 10^{17}$ cm^{-3} and the degree of compensation $K \approx 0.7$ from [81]. Noteworthy is the sharp change, almost a kink, in the curve at $T \approx 17$ K, indicating a possible SFT. The SFTs corresponding to a sharp change in the amplitude of spin fluctuations are considered in more detail in the next subsection.

We also note that the above example does not exhaust the options for studying SFTs in semiconductors. In particular, study [84], where CVD diamond plates were studied by EPR, is of interest. In this material, a spin glass state of radiation defects emerged after irradiation with neutrons. Interestingly, a fluctuation change in the g-factor was discovered in such a system, and the idea of the formation of ferron-type spin-polaron states was used to explain the observed effects [84]. Yet another promising semiconducting material for studying spin fluctuation phenomena will perhaps be Si:P, in which weak ferromagnetism was discovered [85].

4.3 Spin fluctuation transitions accompanied by a sharp change in the amplitude of spin fluctuations with varying temperature ($Hg_{1-x}Mn_xTe$ and MnSi)

A step-wise change in the EPR linewidth with varying temperature was discovered when studying the magnetic

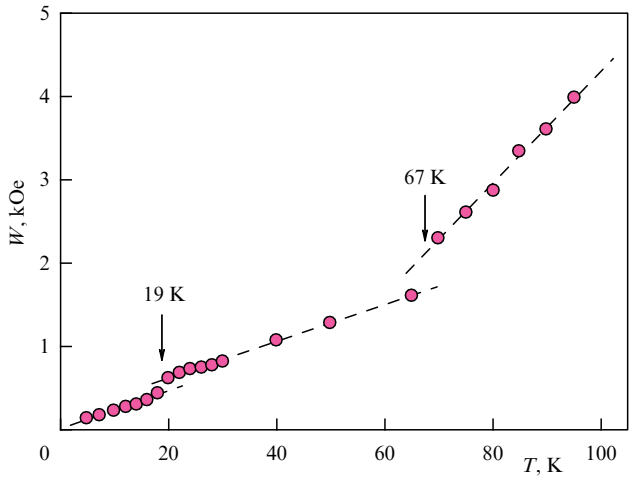

Figure 14. EPR linewidth in magnetic semiconductor $Hg_{0.865}Mn_{0.135}Te$ [86]. At two characteristic temperatures of 67 K and 19 K, temperature dependence exhibits jumps that can be associated with SFTs.

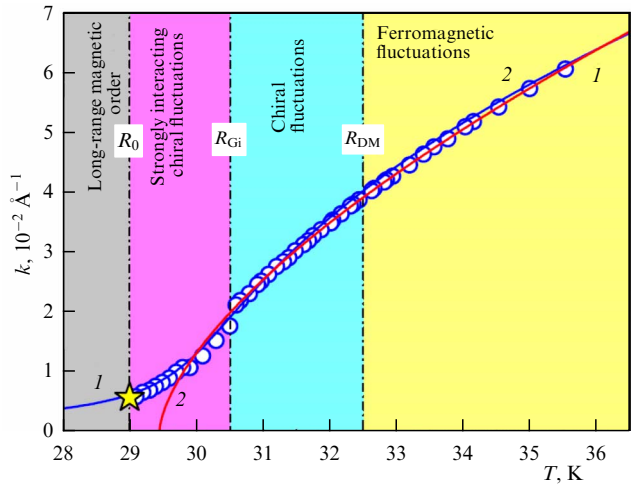

Figure 15. Temperature dependence of inverse correlation length for MnSi (circles) from [39] and various theoretical approximations: *1* — Brazovskii's theory of helical magnets (Eqn (5)); *2* — standard critical behavior (Eqn (4)). Regions of ferromagnetic fluctuations, helical (chiral) fluctuations, strongly interacting chiral fluctuations, and the helical phase with long-range magnetic order are shown according to the description proposed in [39]. Star indicates the inverse correlation length that corresponds to the helix pitch in the helical phase. (From [88].)

semiconductor $Hg_{0.865}Mn_{0.135}Te$ [86]. Measurements were carried out using an X-band spectrometer at a frequency of 9.36 GHz. Three lines were observed in the experiment, caused by different configurations of magnetic manganese ions in the HgTe matrix [86]. In Fig. 14, we show the temperature dependence $W(T)$ of the EPR line with the maximum width for which the largest spin fluctuation contribution can be expected. A sharp change in $W(T)$ occurs at $T \approx 67$ K and $T \approx 19$ K, and pronounced features of the remaining lines are also observed at the same temperatures [86].

Because $Hg_{0.865}Mn_{0.135}Te$ has no magnetic ordering in the temperature range under consideration, the observed jumps in $W(T)$ can apparently be caused by SFTs that occur in the paramagnetic phase. We note that the $Hg_{1-x}Mn_xTe$ system is a classic example of a system with spin polarons [87] and is therefore characterized by a 'natural' general mechanism for the occurrence of spin fluctuations (see Section 2.1 and Fig. 1). Nevertheless, it remains unclear from [86] what exactly happens to spin polarons in $Hg_{1-x}Mn_xTe$ in the range of a sharp change in the EPR linewidth.

We now consider the behavior of spin fluctuations in the paramagnetic phase of another system with spin polarons: the strongly correlated metal MnSi. For single crystals of this helical magnet, detailed data are available both on the temperature dependence of the correlation length extracted from SANS experiments [39] and on the EPR linewidth measured at a frequency of ~ 60 GHz [37]. The results of these independent experiments were compared in [88].

It is convenient to start the analysis with the temperature dependence of the inverse correlation length $k(T) = 1/R_c(T)$ (Fig. 15). To explain the experimental results, Brazovskii's theory generalized to the case of helical magnets was used in [39]. As noted above, the possibility of SFTs is not taken into account in this approach; however, several spin fluctuation regimes arise that smoothly transform one into another. The crossover region between different types of spin fluctuations is determined from the condition $R_c \sim R_i$, where R_i is the spatial scale associated with a certain type of interaction in the system (see Section 2.2). Thus, the domains of ferromagnetic, chiral, and strongly interacting chiral fluctuations can be considered in the paramagnetic phase of MnSi (see Fig. 15).

If we use expression (5) for the inverse correlation length, then the approximation of the experimental data depends on three parameters: T_{MF}, T_0, and k_{Gi}. But if the parameter T_{MF} is fixed, then the point $k(T_{MF}) = k_{Gi}$ on the curve $k(T)$ is actually fixed, and the only adjustable parameter is the smearing temperature T_0. If we additionally require the condition $k(T_c) = 1/R_0$ to hold for the helix pitch in the helical phase, then T_0 can be considered fixed. For $R_0 = 180$ Å [39], this procedure provides a good description of the experimental dependence $k(T)$ with the parameters $T_{MF} = 30.5$ K, $k_{Gi} = 1.9 \times 10^{-2}$ Å^{-1}, and $T_0 = 0.5$ K (curve *1* in Fig. 15).

It is noteworthy that, in the theory under consideration, $k(T)$ remains finite in the entire region $T \geqslant T_c$, while, for a conventional phase transition, the correlation length diverges at the phase transition point (Eqn (4)), and therefore $k(T)$ vanishes [39]. It is interesting that if the standard formula (4) is used to approximate the inverse correlation length of MnSi, then the fit also gives a result that is in good agreement with experiment at the parameters $T_{MF} = 29.44 \pm 0.02$ K, $\nu = 0.64 \pm 0.06$, and $k_0 = (2.19 \pm 0.02) \times 10^{-3}$ Å^{-1} (curve *2* in Fig. 15). Formula (4) then describes experiment in the range $T > 30$ K, and deviations from theoretical dependence (4) in the range $T_c < T < 30$ K can be associated with the formation of intermediate spin-polaron phases that can arise during the paramagnet–ferromagnet phase transition [89] and (or) with SFTs. Thus, a description of the temperature dependence of the inverse correlation length for MnSi can be obtained in the framework of various models.

However, the picture of a smooth change in the correlation length, although consistent with the standard description of a magnetic phase transition, is incomplete. To identify spin fluctuation features, it is convenient to consider the temperature derivatives of the inverse correlation length $\partial k/\partial T$ and of the EPR linewidth $\partial W/\partial T$ [88]. From a comparison of the data on $\partial k/\partial T$ and $\partial W/\partial T$, it is clear that, at certain temperatures, MnSi exhibits a sharp change in the parameters of spin fluctuations: their amplitude and (or) frequency

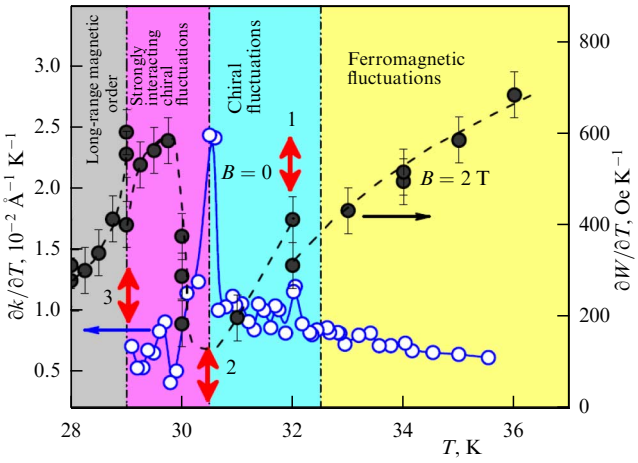

Figure 16. Temperature dependences of derivatives of inverse correlation length $\partial k/\partial T$ and of EPR linewidth $\partial W/\partial T$ for MnSi (initial experimental data taken from [37, 39]). Notation for fluctuation regions is the same as in Fig. 15. Arrows 1–3 show various spin fluctuation transitions. (From [88].)

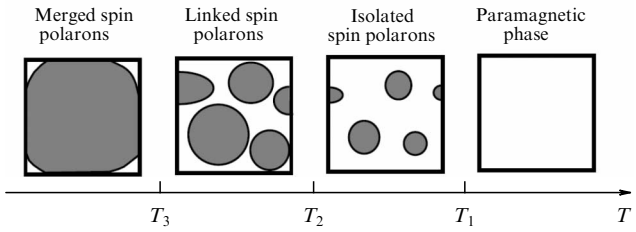

Figure 17. Evolution of spin-polarized phases with temperature according to [89].

defined by the width of the EPR line, as well as the spatial scale (correlation length), acquire features at almost identical temperatures (Fig. 16). Because the $k(T)$ data were obtained in a zero magnetic field [39], and the EPR linewidth corresponds to the resonant field ~ 2 T [37], such a correspondence of the data indicates that, in the considered domain of the temperature–magnetic field parameters, MnSi undergoes several SFTs, and the corresponding boundaries on the magnetic phase diagram are almost vertical.

Let us first note features at $T = 32$ K (arrow 1 in Fig. 16: a jump in the derivative $\partial W/\partial T$ and a maximum of $\partial k/\partial T$). This SFT1 is observed in the temperature range where helical fluctuations occur, according to [39]. But, in contrast to the model description in [39], the experiment shows that the transition between ferromagnetic and helical (chiral) fluctuations in MnSi occurs via a sharp change in spin fluctuation characteristics and is not a crossover.

The strongest change in $\partial W/\partial T$ and $\partial k/\partial T$ and the corresponding SFT2 occurs at $T = 30.5$ K, i.e., according to [39], at $T = T_{MF}$ (arrow 2 in Fig. 16). The transition presumably related to an increase in the interaction of helical fluctuations is therefore not smooth, as was assumed in [39], but is a typical SFT. We note that the features of $\partial W/\partial T$ and $\partial k/\partial T$ at $T \sim T_{MF}$ imply the presence of steps in the temperature dependences $W(T)$ and $k(T)$ (in agreement with the data shown in Fig. 15 and the temperature dependence of the EPR linewidth given in [37]). In view of the previously described results for the $Hg_{1-x}Mn_xTe$ system, we can conclude that such steps are a characteristic feature of magnetic transitions in spin polaron systems.

At temperature $T = 29$ K, equal to the critical temperature T_c in a zero magnetic field, a jump in the derivative $\partial W/\partial T$ is observed (arrow 3 in Fig. 16). The discontinuity of $\partial W/\partial T$ corresponds to a break in the $W = f(T)$ curve, which can be associated with another SFT. Thus, the magnetic transition from the paramagnetic phase to the magnetically ordered phase in MnSi has a very complex nature and occurs via several successive SFTs [88].

Interestingly, three successive transitions that occur with decreasing temperature in a system of spin polarons were predicted by Yu and Min [89]. This approach was applied to the description of the paramagnet–ferromagnet magnetic transition in EuB_6 [89]. In the framework of the proposed model, the evolution of a magnetic system made of LMMs and conduction electrons is understood as the emergence of an inhomogeneous magnetic spin-polaron state and the subsequent change in its spatial characteristics (Fig. 17). Initially, at $T = T_1$, isolated spin polarons form, which exist up to $T_2 < T_1$. At $T \leqslant T_2$, the size and number of spin polarons in the system increase so much that they can no longer be considered isolated, and a range of existence of linked spin polarons arises. With a further decrease in temperature to $T = T_3 < T_2$, the spin polarons begin to touch each other, and a phase of merged spin polarons is formed, which is identified in [89] with a ferromagnetic phase with long-range magnetic order (see Fig. 17). Thus, the approach under consideration not only takes the hierarchy of interactions in the system into account but also includes the change in topology in the system of spin polarons.

It is not inconceivable that the SFTs observed in the paramagnetic phase of $Hg_{1-x}Mn_xTe$ and MnSi are associated with the Yu–Min transitions. In this case, the maximum SFT temperature should be associated with the formation of spin polarons. However, neither the spatially homogeneous model [39] nor inhomogeneous magnetic states [89] account for the experimentally observed sharp change in the characteristics of spin fluctuations during SFTs.

4.4 Spin-fluctuation transitions on the magnetic phase diagram of substitutional solid solutions $Mn_{1-x}Fe_xSi$

We have shown that MnSi-type helical magnets are promising subjects for the search and study of SFTs. In substitutional solid $Mn_{1-x}Fe_xSi$ solutions, which are also metals, the $B-T$ [90, 91] and $T-x$ [49, 53, 90] magnetic phase diagrams exhibit so-called intermediate magnetic phases. Historically, these phases were regarded as domains with specific spin fluctuations [39] or disordered magnetic phases with intermediate (short-range) magnetic order, corresponding to ordered domains 10–50 nm in size [52]. From the standpoint of modern SFT problems, the 'alternative' approaches to the description of intermediate phases [39, 52] are nothing more than a terminological distinction. Indeed, it was already noted in [52] that the neutron diffraction pattern in intermediate phases of $Mn_{1-x}Fe_xSi$ is identical to diffraction data for classical liquid crystals. This observation is fully consistent with the spin nematic model [45], and therefore the appearance of the intermediate phases under consideration should be associated with an SFT.

Features of various physical properties necessary for constructing the $T-x$ magnetic phase diagram of $Mn_{1-x}Fe_xSi$ are extracted from magnetic susceptibility data, neutron scattering, and magnetization analysis in Belov–

Arrott coordinates [49, 52, 53, 90, 91]. The dependence of the derivative of the magnetic susceptibility $\partial\chi/\partial T$ allows finding the temperature of the transition to a phase with long-range magnetic order and the SFT temperature (see Fig. 6). We note that there is a problem in comparing data obtained by different authors, because the nominal composition specified during synthesis is used to identify samples in most studies, but the actual content of elements in the resulting crystals may differ significantly from the nominal one. In this regard, we next consider data in [49], where not only the actual iron content was experimentally determined but also the stoichiometry in the samples was controlled.

To describe the $T-x$ magnetic phase diagram of $Mn_{1-x}Fe_xSi$, the model proposed in [49] turned out to be the most successful (see Section 2.5). When analyzing the magnetic phase diagram, it is necessary to keep in mind that, in the $Mn_{1-x}Fe_xSi$ system, the replacement of manganese with iron dilutes the magnetic subsystem of manganese ions, and hence both structural and magnetic disorders are related to a change in composition. If the iron content in the samples is not too high, it can be assumed in the first approximation that the control parameter x that specifies the magnetic disorder in the model is proportional to the concentration of iron. Then, the temperatures of SFTs following from Eqn (12) can easily be compared with experiment, if we take into account that the temperature of transition to the helical phase $T_c(x)$ decreases in accordance with the linear law $T_c(x) \sim (x - x^*)$, where $x^* \approx 0.11$ [49]. Because the dependence $T_c(x)$ is given and the SFT temperature in the range $x < x^*$ is known for at least one composition, it follows from Eqn (12) that, to describe the diagram, it suffices to take the energy scale for quantum fluctuations $T_2(0)$ and the percolation point x_c as fitting parameters.

The results of modeling the $T-x$ magnetic phase diagram for the critical exponent $\nu_1 = 1/2$ are shown in Fig. 18a. It can be seen that the proposed approach yields quite satisfactory agreement with experiment. We note that the Belov–Arrott analysis yields SFT temperatures (triangles in Fig. 18a) that exceed the SFT temperatures deduced from the magnetic susceptibility data (squares in Fig. 18a), and this difference is most pronounced in the range of small x, including at $x = 0$ (pure MnSi). We assume that the Belov–Arrott analysis gives the temperature at which ferromagnetic correlations are established outside the temperature range in which SFTs were considered in Section 4.3. Within the Yu–Min scenario, the maximum SFT temperature can be associated with the appearance of isolated spin polarons, because their formation is accompanied by the appearance of a specific mechanism of spin fluctuations (see Fig. 1). In addition, it is obvious that the model under consideration is too simple to fully describe the entire complex sequence of SFTs that can occur in a manganese monosilicide (see Section 4.3).

It is clear from Fig. 18a that the model allows describing both SFT1 associated with classical fluctuations (line *1*) and SFT2, which is presumably due to quantum fluctuations (line *2*). As already noted in Section 2.5, the coexistence of classical and quantum fluctuations leads to the appearance of another SFT (SFT3) in the paramagnetic phase (P) at $T_{eq}(x)$ (dashed line *3*). Moreover, the position of this feature on the $T-x$ diagram is determined automatically without the use of any additional parameters [49]. This transition separates the regions where classical fluctuations or quantum fluctuations dominate (the respective CF region on the left and QF region on the right of curve *3* in Fig. 18a). The existence of SFT3 was

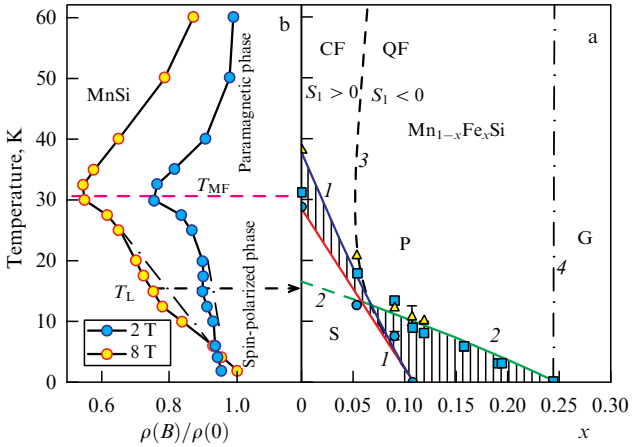

Figure 18. (a) Magnetic phase diagram of substitutional solid solutions $Mn_{1-x}Fe_xSi$ according to data in [49]. Dots show the experiment and lines, a theoretical model. Helical phase S and paramagnetic phase P are indicated. Lines *1* and *2* show boundaries of intermediate states arising due to SFTs associated with classical (line *1*) and quantum (line *2*) fluctuations. Dashed line *3* in the paramagnetic phase corresponds to the SFT between classical (CF) and quantum (QF) fluctuations. Line *4* denotes the Griffiths-phase boundary. (b) Temperature dependences of the magnetoresistance of MnSi in fixed magnetic fields of 2 T and 8 T. Main minimum of magnetoresistance corresponds to the boundary between the paramagnetic phase and the spin-polarized phase (according to [25]).

experimentally confirmed by data on the temperature dependence of the resistivity $\rho(T, x)$ [92] and the results of studying the anomalous Hall effect [93]. In particular, it was shown in [93] that, due to a change in the nature of magnetic scattering on spin fluctuations in the expression for the anomalous contribution to the Hall resistance $\rho_{aH} = S_1\rho M$, proportional to the magnetization M, the coefficient S_1 changes sign when crossing the CF – QF borderline (Fig. 18a).

The three SFTs considered above, which follow from the model in [49], do not exhaust the spin-fluctuation phenomena that can be observed in the $Mn_{1-x}Fe_xSi$ system. It was found that, in the region $x \geqslant x_c \sim 0.24$, the minimum on the curve $\partial\chi/\partial T = f(T)$ corresponding to an SFT is not observed and $T_2(x)$ vanishes. Thus, the value of x_c is known from experiment and the quantitative description of the $T-x$ diagram essentially depends on one parameter, $T_2(0)$. At the same time, at $x \geqslant x_c$, the nature of the temperature dependence of the magnetic susceptibility changes. In [49], the magnetic susceptibility in that range of iron concentrations was found to depend on temperature according to a power law

$$\chi(T) \sim \frac{1}{T^{\xi}} \tag{19}$$

with the exponent $\xi = 0.5-0.6$. This behavior is typical of the disordered Griffiths phase formed by spin clusters in a system with a power-law distribution of exchange integrals [94, 95]. For $x < x_c$, there are no clusters in the system, but there are fluctuations, and spin clusters appear in the range $x \geqslant x_c$, and it is therefore natural to assume that the spin fluctuations freeze out on line *4* (see Fig. 18), which is accompanied by an abrupt change in their characteristic frequency. Thus, the results in [49] suggest the presence of another SFT type, a dynamical one. This hypothesis is qualitatively consistent with the results of a study of the frequency of spin fluctuations

[53], according to which features in $\Gamma(T)$ can arise under an SFT (see Fig. 7).

Dynamical SFTs can also be associated with specific points on the $T-x$ magnetic phase diagram. The model in [49] was built under the assumption of the existence of two singular points, the first of which, $x^* \sim 0.11$, is the vanishing point of $T_c(x)$, the temperature of transition to the helical phase with long-range magnetic order. As the temperature decreases along the $x = x^*$ line, SFT2 occurs first, and therefore such a singular point can be classified as a quasi-hidden quantum point. The second singular point $x = x_c$ corresponds to the vanishing of the temperature $T_2(x)$; however, from the theoretical standpoint, it is not clear whether it can be considered a quantum critical point [50]. At the same time, in [96], for $Mn_{1-x}Fe_xSi$ samples with $x = x^*$ and $x = x_c$, in contrast to all other compositions, a particular temperature dependence of the linewidth $W(T)$ was discovered, which can be quantitatively interpreted in the framework of a theoretical description of spin relaxation in a quantum critical regime [55]. Thus, the results in [96] show that an SFT with a change in spin dynamics can occur at the quantum critical point.

To conclude this section, we note that describing the $T-x$ magnetic phase diagram of substitutional solid solutions $Mn_{1-x}Fe_xSi$ requires taking frustration effects into account [93]. As was shown in [93], magnetic interactions in this system cannot be completely described in the framework of a simple model that includes only the ferromagnetic interaction and Dzyaloshinskii–Moriya interactions between manganese ions (Eqn (3)). The reason for this is that the exchange interaction between LMMs of manganese is the Ruderman–Kittel–Kasuya–Yoshida (RKKY) interaction via band carriers, and hence, in addition to the leading nearest-neighbor exchange energy J_1, the interaction energy J_2 between next-to-nearest neighbors must be taken into account [93]. In $Mn_{1-x}Fe_xSi$, depending on the iron content, the concentrations of electrons and holes modulating the RKKY exchange vary, giving rise to a nontrivial behavior of $J_1(x)$ and $J_2(x)$. Thus, the exchange energy $J_1(x)$ decreases as x increases and changes sign at $x \approx 0.17$, which corresponds to a change in the type of magnetic interaction from the ferromagnetic to the antiferromagnetic one. In contrast to $J_1(x)$, the exchange energy $J_2(x)$ weakly depends on x and corresponds to antiferromagnetic interaction in the entire range $x \leqslant 0.26$ [93]. As follows from Fig. 18a, the temperature of transition to the helical phase $T_c(x)$ vanishes at $x^* \sim 0.11$, i.e., at the iron concentration for which the main ferromagnetic exchange is nonzero. However, in the vicinity of $x^* \sim 0.11$, the conditions $|J_1(x)| \approx |J_2(x)|$ and $J_1(x)J_2(x) < 0$, characteristic of strong frustration, are satisfied. It is assumed in [93] that precisely the frustration effects caused by competing types of magnetic interactions with energies $J_1(x)$ and $J_2(x)$ lead to the suppression of the helical phase at the iron concentration $x^* \sim 0.11$, which is less than $x \approx 0.17$ corresponding the vanishing of $J_1(x)$. Curiously, in the neighborhood of the second singular point $x_c \sim 0.24$, the relation $|J_1(x)| \approx |J_2(x)|$ is again valid for $Mn_{1-x}Fe_xSi$, but in this case both exchange energies are of the antiferromagnetic type [93]. It is easy to see that the neighborhood of x_c also corresponds to strong frustration when the interactions $J_1(x)$ and $J_2(x)$ tend to orient the LMMs in opposite directions. Apparently, frustration in the $Mn_{1-x}Fe_xSi$ system is also responsible for the position of the percolation threshold. Indeed, at $x_c \sim 0.24$, from a geometric standpoint,

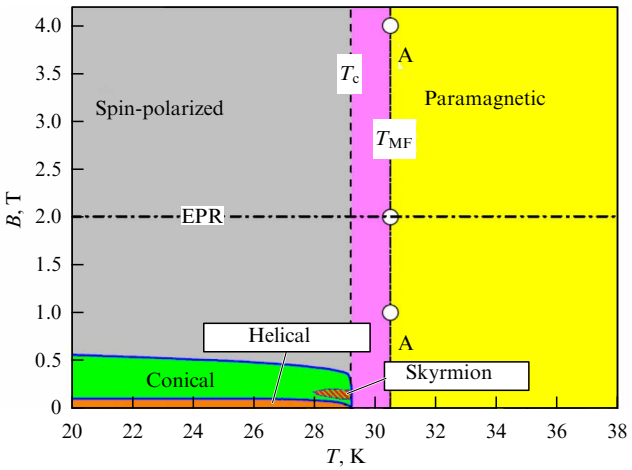

Figure 19. Magnetic phase diagram of MnSi. Paramagnetic, helical, skyrmion, and spin-polarized phases are indicated. Dashed line is extrapolated line $T_c(B = 0) = \text{const}$. Three-dotted line (EPR) corresponds to the magnetic field in which the EPR was studied. White dots (line A–A) represent the magnetic transition temperatures extracted from magnetic scattering data. Region inside the spin-polarized phase preceding the spin-polarization transition at $T \sim T_c$ is shown in pink. (From [25].)

an infinite cluster of manganese LMMs is preserved in the structure of the solid solution. However, the frustration effect can apparently enhance the tendency toward magnetic inhomogeneity of $Mn_{1-x}Fe_xSi$, and, at $x \geqslant x_c \sim 0.24$, can stimulate the decay of the magnetic subsystem of solid solutions into individual clusters that make up the Griffiths phase [93].

Thus, using the example of SFT2, we see that frustration can affect an SFT. Frustration, in turn, can also affect spin fluctuations in the system. However, the details of the relation between frustration and SFTs remain unclear. It cannot be ruled out that theoretical and experimental study of this problem would represent a promising task for further research.

4.5 Spin fluctuation transition in the magnetically ordered MnSi phase

The SFTs described above occur in magnetic phases in which long-range magnetic order is either absent (the paramagnetic phase) or hidden (the quadrupole-order phase). In addition, an SFT apparently also occurs at the magnetic transition point. It is appropriate to ask whether an SFT is possible in a magnetically ordered phase. A possible answer to this question was obtained in a recent study [37] where EPR in single crystals of manganese monosilicide was investigated.

We first consider the magnetic-phase $B-T$ diagram of MnSi, constructed in accordance with the data in [25] and with the literature data presented in that paper (Fig. 19). In a zero magnetic field $B = 0$ at $T_c \sim 29$ K, a transition occurs from the paramagnetic phase to the helical phase. An increase in the magnetic field in the range $T < T_c$ leads to rapid suppression of the helical phase and the formation of a mixture of domains from conical phases. A further increase in the magnetic field leads to a reorientation of the domains, resulting in the formation of a conical phase with the cone axis directed along the magnetic field. At $B \sim 0.5$ T, the conical phase turns into an analogue of the ferromagnetic phase — a spin-polarized phase in which the magnetic moments are aligned in parallel. All magnetically ordered phases in Fig. 19

represent different spin-polarized phases, and, in addition, spin polarons can exist in some range in the paramagnetic phase ($T > T_c$). A possible exception to the set of spin-polarized phases may be a small pocket in the vicinity of T_c formed by the skyrmion phase (or, according to the terminology used in the literature, the A-phase), which in turn has an internal structure [97].

The spin-polaron nature of the various magnetic phases in MnSi is of fundamental importance for understanding the physics of the transition between the paramagnetic and spin-polarized phases. For a standard ferromagnet in a nonzero magnetic field, there is no phase transition between the paramagnetic and ferromagnetic phases [1], and we can only talk about a greater or lesser degree of LMM ordering depending on temperature. As follows from the analysis of experimental data on magnetization and magnetoresistance performed in [25], the transition between the paramagnetic and spin-polarized phases of MnSi is abrupt. It was established in [25] that the position of a wide minimum on the temperature dependence of magnetoresistance at $B = \text{const}$ (Fig. 18b) corresponds to some well-defined temperature that coincides with T_{MF} within the experimental error (line A–A in Fig. 19), which is due to the peculiarities of magnetic scattering in this material [25]. For spin-polarized phases, the standard restriction [1] on the paramagnet–ferromagnet transition is lifted and, according to [25], it is at the A–A boundary that the reduced magnetic moments of spin polarons are ordered.

In [25], in addition to the main magnetoresistance minimum in the range of existence of the spin-polarized phase, an additional minimum was discovered at $T_L \sim 15$ K (Fig. 18b). The nature of this anomaly had had no explanation until recently; however, it follows from the data in Fig. 18b that the temperature T_L corresponds surprisingly well to the characteristic SFT temperature on quantum fluctuations $T_2(x)$, extrapolated to $x = 0$ (pure MnSi, the green dashed line in Fig. 18a). Thus, the low-temperature magnetoresistance feature of MnSi may reflect a change in the nature of spin fluctuations in the spin-polarized phase of MnSi as a result of some SFT. To test this hypothesis, it is necessary to confirm the change in the nature of spin fluctuations at the relevant temperature, and also to verify that it can indeed be associated with the effect of quantum fluctuations.

A positive answer to the questions posed was obtained in [37], where high-frequency (~ 60 GHz) EPR in MnSi single crystals was studied in the temperature range of 2–40 K in a magnetic field B up to 8 T. For a frequency of ~ 60 GHz, the magnetic resonance field in MnSi is ~ 2 T (see Fig. 19). The focus was on obtaining the most detailed data, for which several temperature scans were performed in the specified interval and about 200 spectra were recorded, yielding a record number of experimental points for the temperature dependences of the linewidth $W(T)$ and the g-factor $g(T)$. To find the derivatives of these parameters with respect to temperature, each scan was processed separately, after which all obtained data were analyzed together on a common graph.

We first consider the temperature dependence of the linewidth. As the temperature decreases, the linewidth first decreases and passes through a minimum at $T \sim 26$ K; then, in the range $T < 26$ K, a significant low-temperature increase in $W(T)$ is observed: as the temperature decreases from $T = 26$ K to $T = 2$ K, the line width more than doubles

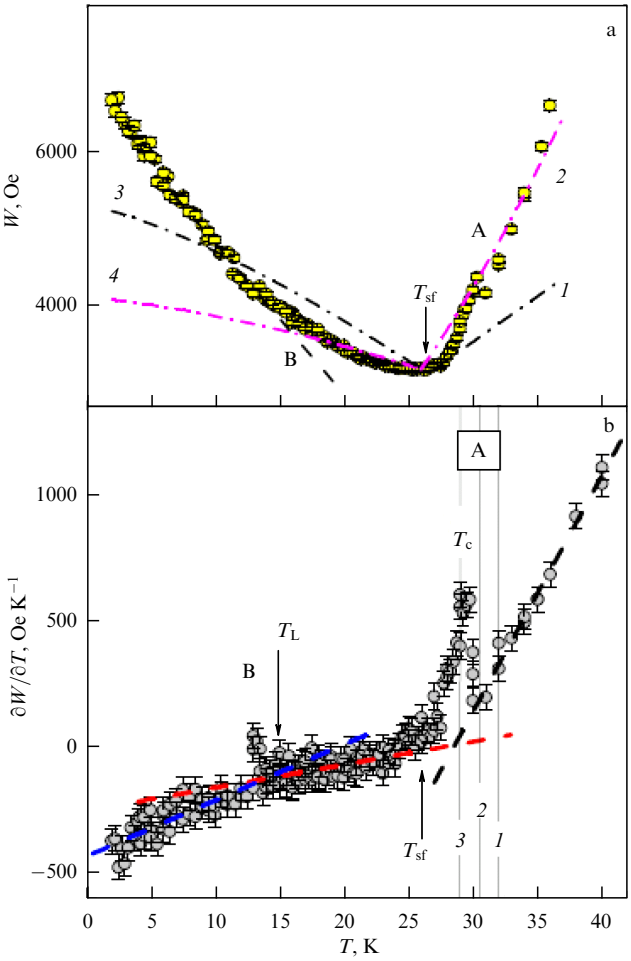

Figure 20. Temperature dependences of (a) EPR linewidth W and (b) derivative $\partial W/\partial T$. Letters indicate features of $W(T)$: a group of SFTs and the transition to the spin-polarized phase (A) and the change in the slope of the $\partial W/\partial T$ curve (B). (a) Dots show the experiment, *1–4* are theoretical dependences. Arrows indicate different characteristic temperatures. (b) Dots show the derivative calculated from experimental data, dotted lines show the qualitative change in derivative $\partial W/\partial T$ in different temperature ranges. Solid lines *1–3* in Fig. b correspond to SFTs *1–3* in Fig. 16. Characteristic temperatures T_c, T_{sf}, and T_L are shown. Figure a shows part of the data restricted to the temperature range below 35 K. (From [37].)

(Fig. 20a). In the range $T > 26$ K, a group of A features is observed (discussed in detail in Section 4.3), which is caused by SFTs and a magnetic transition to the spin-polarized phase (Fig. 20a, b and Fig. 16).

In addition to the jump in the line width on the $W(T)$ curve discussed above, we can identify an anomalous region B in the vicinity of $T \sim T_L \approx 15$ K, where the slope of the $\partial W/\partial T = f(T)$ curve changes by a factor of 2.4 (Fig. 20b). Thus, EPR data indicate that, in the temperature range $13 < T < 17$ K, where an SFT within the spin-polarized phase is expected for MnSi, a change in the nature of spin fluctuations actually occurs. We note that, according to [37], feature B corresponds to a local maximum of the derivative of the linewidth with respect to temperature; however, as can be seen from Fig. 20b, its amplitude is comparable to the magnitude of the error in calculating $\partial W/\partial T$ from experimental data (Fig. 20b).

The observed nonmonotonic dependence $W(T)$ (Fig. 20a) is highly nontrivial. Indeed, for a strongly correlated metal

such as MnSi, a Korringa-type spin relaxation is expected in the paramagnetic phase with $W(T) \sim 1/\chi(T)$, where χ is the magnetic susceptibility [17, 56]. Because the magnetic susceptibility increases as it approaches the point of transition to the quasiferromagnetic spin-polarized phase, the linewidth should decrease, which is indeed observed experimentally (Fig. 20a). In this case, $\chi(T)$ is given by the Curie–Weiss law, and therefore a linewidth dependence of the form $W(T) \sim 1/\chi(T) \sim T - T_c$ should be observed. But the calculation of the derivative $\partial W/\partial T$ shows that this quantity in the paramagnetic range $T > T_c$ is linear in temperature, rather than being a constant (Fig. 20b). As a result, the linewidth $W(T)$ in the paramagnetic phase of MnSi depends on temperature quadratically, and the standard Korringa mechanism of spin relaxation in the range $T > T_c$ can be applicable to the description of experimental data only at a qualitative level. We note that the decrease in the line width with decreasing temperature continues in the range $T < T_c$, down to the minimum point of $W(T)$ at $T = T_{sf} \approx 26$ K (Fig. 20a). If we stay within the 'Korringa paradigm,' we have to assume that the correlations in the MnSi magnetic subsystem are weakened throughout the entire range $T > T_{sf}$, and not only in the paramagnetic phase with $T > T_c$.

This assumption is obviously not valid for the magnetic subsystem formed by conventional LMMs, but it may make sense for a system of spin polarons. We have shown that the process of formation of the spin-polarized phase in MnSi has a complex multistage character and is accompanied by a change in the characteristics of spin polarons. Therefore, the temperature T_c of the transition to a phase with long-range magnetic order and the temperature T_{sf} at which magnetic correlations are enhanced may differ.

In [37], a simple model was proposed to describe the temperature dependence of the EPR linewidth. For spin-polaron states, fluctuations in the magnetic moment were assumed to be caused by transitions of electrons from quasibound states in the vicinity of Mn LMMs to band states. The electron nature of spin fluctuations suggests that the Moriya theory [22] may be promising for solving the problem, and we can use Eqns (1) and (2) for the amplitude of spin fluctuations $S_L(T)$ in a system with ferromagnetic correlations. The function $S_L(T)$ given by Eqns (1) and (2) has a minimum at a characteristic temperature T_{sf}, which is interpreted in [37] as the temperature of ordering the spin fluctuations in the spin-polaron state, in other words, as the temperature of an SFT associated with the electron subsystem of the spin polaron. The spin-fluctuation contribution to the magnetic susceptibility, according to [22], is then inversely proportional to the square of the spin fluctuation amplitude $\chi(T) \sim 1/S_L^2(T)$. The nonmonotonic theoretical dependence $S_L(T)$ is in qualitative agreement with the experimental data for $W(T)$.

Within this approach, for the standard Korringa mechanism at $T > T_{sf}$, the EPR linewidth still depends on the temperature linearly, $W(T) \sim 1/\chi(T) \sim S_L^2(T) \sim T$ (Eqn (1)), which is in poor agreement with experiment (curve *1* in Fig. 20a). The situation can be remedied by a standard linewidth renormalization by some fast process with a characteristic time τ, which alters the nature of phase coherence at resonance [98]: $\tilde{W}(T) = W^2(T)\tau$. Under certain conditions, we can then expect a modified Korringa law $W(T) \sim 1/\chi^2(T) \sim S_L^4(T) \sim T^2$. This estimate for the experimental values of T_{sf} and $W(T_{sf})$ that correspond to a minimum of $W(T)$ demonstrates satisfactory agreement with experiment for $T < T_c$ (curve *2* in Fig. 20a). We note that an alternative interpretation of the quadratic dependence was proposed in [55], where this effect was associated with the relaxation of quasiparticles in heavy-fermion systems, to which manganese monosilicide belongs (according to [99], the effective electron mass of MnSi in the temperature range under consideration is 10 times the free electron mass).

In the range $T < T_{sf}$, the system of spin polarons is ordered and Korringa-type formulas $W(T) \sim 1/\chi(T)$ or $W(T) \sim 1/\chi^2(T)$ are not applicable. In the magnetically ordered phase, an option for taking the spin-fluctuation contribution like $W(T) \sim S_L^2$ into account, considered in Section 3.2, is also invalidated because the range of applicability of the corresponding correction is limited by the paramagnetic phase. From Figure 20a, we can clearly see that the dependence $W(T) \sim S_L^2$ is in poor agreement with experiment in the entire range $T < T_{sf}$ (curve *3*). Therefore, the following version of the description of the temperature dependence of the EPR linewidth in a magnetically ordered phase was proposed in [37]. If ΔM is the amplitude of magnetization fluctuations along the external field direction, then, in the absence of correlations between fluctuations in the spin precession frequency and magnetization, we can assume that $W(T) = \Delta M/(\partial M/\partial B) \sim S_L(T)$. This approximation is in good agreement with experiment down to $T_L \sim 15$ K (curve *4* in Fig. 20b). In the low-temperature range $T < T_L$, additional line broadening occurs that cannot be described using the model function $S_L(T)$ for $T < T_{sf}$ (Eqn (2)). It follows from Fig. 20a that, at $T \sim 2$ K, the experimental value of the line width is 1.6 times larger than expected from the model calculation. As noted above, in the vicinity of $T \sim T_L$, the dependence $\partial W/\partial T = f(T)$ experiences a significant change (Fig. 20b). Thus, both the experimental data and their theoretical analysis are consistent with the idea of a change in the nature of spin fluctuations in the vicinity of the temperature of the assumed low-temperature SFT in MnSi.

We next analyze the temperature dependence of the *g*-factor. The temperature dependences of $g(T)$ and of the derivative $\partial g/\partial T = f(T)$ obtained in [37] (Fig. 21) provide additional information about the decisive role of spin fluctuations in generating low-temperature dynamical magnetic properties of MnSi. It is clear from Fig. 21a that the *g*-factor first increases with decreasing temperature, passes through a maximum at $T \sim 5$ K, and then starts decreasing in the range $T < 5$ K. The group of A features (the vicinity of the transition between the paramagnetic and spin-polarized phases) appears in the form of a break in the curve $\partial g/\partial T = f(T)$ (Fig. 21b), while feature B (the SFT expected at T_L) cannot be identified to within the error on the temperature dependences $g(T)$ and $\partial g/\partial T$ (see Fig. 21). We note that the characteristic temperature T_{sf} corresponding to the EPR linewidth minimum cannot be associated with any pronounced changes in the temperature dependence of the *g*-factor or its derivative either.

According to [37], the initial growth part of the *g*-factor with decreasing temperature in the range $T > T_c$ can be associated with a change in the local field in the vicinity of the manganese ion in the paramagnetic phase due to a change in the LMM screening by band electrons in the process of rearrangement of the system of spin polarons. To estimate the effective value of the spin polaron *g*-factor g_S in the limit $T \to 0$, we can use the results for a two-sublattice ferrimagnet [100] in the configuration of oppositely directed magnetic

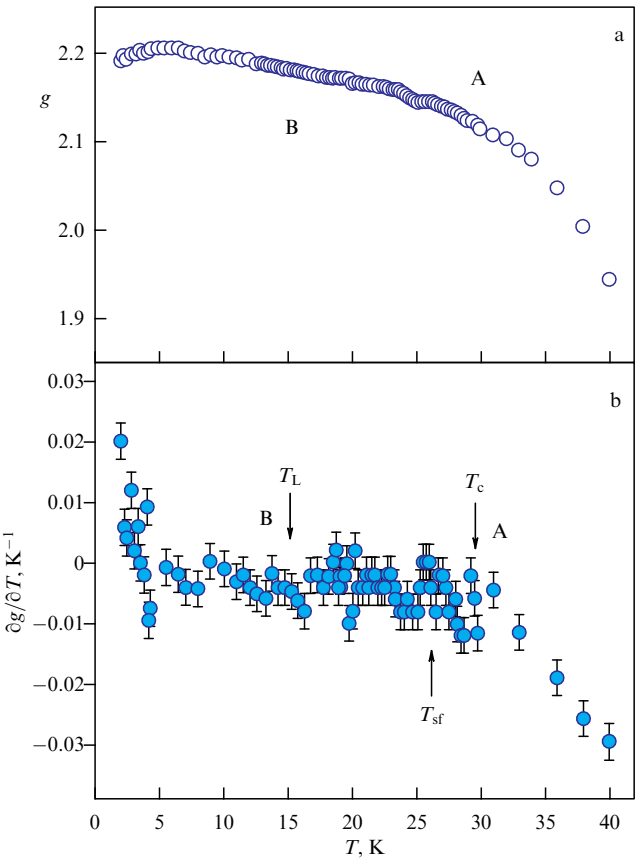

Figure 21. Experimental temperature dependences of (a) the g-factor and (b) the derivative $\partial g/\partial T$. Features and characteristic temperatures following from the temperature dependence of the EPR linewidth are noted (notation is the same as in Fig. 20). Error in determining the g-factor in Fig. a corresponds to the size of an experimental point. (From [37].)

moments of electrons μ_e and manganese LMMs μ_{Mn} in the spin-polaron state [29],

$$g_S = \frac{g_e\mu_e n_e - g_{Mn}\mu_{Mn}n_{Mn}}{\mu_e n_e - \mu_{Mn}n_{Mn}} \approx g_{Mn}\frac{g_e\mu_{Mn}/g_{Mn}\mu_e - 1}{\mu_{Mn}/\mu_e - 1}, \quad (20)$$

where n_e and n_{Mn} are the numbers of electrons and LMMs in a spin polaron. In (20), we used the relation $n_e/n_{Mn} \approx (\mu_{Mn}/\mu_e)^2$ obtained in [29] as the spin polaron stability condition. To obtain an estimate, we assume that the g-factor of electrons is $g_e \approx 2$, and use the high-temperature value in the paramagnetic phase for the g-factor of Mn, $g_{Mn} \approx 1.9$ (Fig. 21a). For $\mu_e = \mu_B$ and $\mu_{Mn} = 1.3\mu_B$ [29], we can then use Eqn (20) to find $g_S(T \to 0) \approx 1.23g_{Mn} \sim 2.3$. Thus, in the SP phase, in which spin-polaron states form at $T < T_c$, it is natural to expect an increase in the g-factor with decreasing temperature in accordance with the observed behavior (Fig. 21a). Moreover, our numerical estimate $g_{SP}(T \to 0) \sim 2.3$ is also in reasonable agreement with experiment.

The decrease in the g-factor observed at $T < 5$ K (Fig. 21a), first, indicates the presence of an additional particular contribution to $g(T)$. Second, the decrease in $g(T)$ occurs in the range where the dependence $W(T)$ changes, which can also be associated with an additional contribution to the linewidth. This behavior is consistent with the predictions in [57] (Section 3.2, Eqns (14) and (15)) that taking quantum fluctuations of the magnetic moment into account gives rise to a renormalization of the parameters in the Landau–Lifshitz equation, as a result of which the EPR linewidth and the resonance field change. Quantum spin fluctuations act to simultaneously increase W and decrease g, which is in qualitative agreement with experimental results in the range $T \leqslant T_L \sim 15$ K (see Figs 20 and 21).

Thus, the set of EPR data for $W(T)$ and $g(T)$ obtained in [37] is consistent with the idea of an SFT in the vicinity of $T_L \sim 15$ K associated with quantum fluctuations. These data confirm the possibility of the existence of an SFT in a magnetically ordered (spin-polarized) phase in MnSi, which significantly extends the range of applicability of the SFT concept.

5. Conclusions

According to our observations, at a certain stage in its development, any field of research goes through a phase of being 'written in stone,' when exhaustive definitions are given and maxima are stated that practically take the form of aphorisms. It is difficult to resist the temptation and not quote one of the books written in the middle of the last century, according to which a "fundamental feature of the magnetic properties of matter is the coexistence and 'struggle' of mutually opposite phenomena: paramagnetism and diamagnetism, paramagnetism and antiferromagnetism, and ferromagnetism and antiferromagnetism. Only a thorough study of this struggle allows revealing the connection between magnetic properties and structural features" [101].

This review will hopefully allow the reader to conclude that, while the above 'struggle' of classical concepts was under way, a new group of magnetic phenomena took center stage, the SFTs. Spin fluctuation transitions clearly manifest themselves as a sharp change in the characteristics of spin fluctuations, observed via electron paramagnetic resonance and SANS methods. This group of magnetic phenomena can occur both in magnetically ordered phases and in phases without magnetic order or with a hidden magnetic order.

Systematic research into SFTs is just beginning. Nevertheless, the available experimental data and theoretical results allow outlining an approximate classification of SFTs:

Disorder–disorder SFT. Transitions of this type reflect a change in the nature of magnetic fluctuations in the paramagnetic phase of magnetic semiconductors $Hg_{1-x}Mn_xTe$ and helical magnets based on MnSi. Such SFTs can be diagnosed by changes in magnetization and magnetic susceptibility, EPR, and neutron scattering patterns and are therefore often described as phases with intermediate magnetic order (the magnetic analogue of a liquid or amorphous phase). From a theoretical standpoint, describing the SFT in MnSi and $Mn_{1-x}Fe_xSi$ requires taking the coexistence of classical and quantum fluctuations into account.

A study of the disordered Ising model showed the emergence of an SFT that consists of a sharp change in the amplitude of spin fluctuations and the exchange energy distribution function when the concentration of magnetic centers randomly located in space changes. Interestingly, SFTs of this type occur for both ferromagnetic and antiferromagnetic exchange. Doped semiconductors may be promising subjects for testing theoretical predictions.

Disorder–hidden (*quadrupole*) *order SFT*. This is a magnetic transition to the spin nematic phase, under which the anisotropy of spin fluctuations changes. In the paramagnetic phase, the average spin at a site is zero, and spin fluctuations

(average squared spin) are identical in all directions. With the transition to a phase with quadrupole order, the average spin is still zero, but the average squared spin is different along different directions. The spin nematic effect was discovered in the antiferroquadrupole phase of CeB_6 by studying the angular dependences of EPR and magnetoresistance.

Orientation SFT consists of changes in the preferred direction of anisotropic spin fluctuations. It was experimentally observed in the antiferroquadrupole phase CeB_6 with varying temperature.

Order–order SFT. EPR studies have allowed detecting an SFT caused by quantum fluctuations at $T \sim 15$ K in the magnetically ordered (spin-polarized) phase of MnSi. It is noteworthy that this SFT occurs at a temperature significantly lower than the transition temperature to the magnetically ordered phase (~ 30 K) and is outside the region of classical fluctuations.

Currently, the set of experimental examples in which SFTs have been analyzed includes highly correlated metals, magnetic semiconductors, and even a classical semiconductor, doped germanium. It seems very likely that all these systems are united by the presence of spin-polaron effects. A spin polaron is a quasibound state formed by several conduction electrons and LMMs in a crystal. At a qualitative level, such an object seems very convenient for describing the mechanism of the occurrence of spin fluctuations and SFTs in a wide variety of materials. Another type of system where strong spin fluctuations and the associated SFTs can also occur are frustrated systems. Unfortunately, SFTs in frustrated systems have not been studied in sufficient detail.

A careful study of SFT problems allows expecting them to be detected in a wide variety of systems, including very exotic ones. Candidates include a nematic-type transition inside the skyrmion phase (A-phase) of MnSi [97] and a magnetic transition at $T \sim 5$ K on the surface of a strongly correlated topological insulator SmB_6 [17, 102].

The detection of SFT has become possible due to the development of experimental methods, primarily EPR and SANS. Their improvement has allowed going beyond the classically recognized 'smooth' dependences of the correlation length and width of the EPR line. As a result, a window of opportunity opened for experimenters to observe a sharp change in the parameters of spin fluctuations that is outside the standard theory of phase transitions. Because the data obtained indicate the limitations and incompleteness of the existing models of magnetic phase transitions, we hope that studies of SFTs will serve as a stimulus for further development of theoretical concepts. As a promising avenue, we note the description of phase transitions using a multicomponent order parameter and models of phase transitions in liquids and glasses [103]. This is supported by a certain similarity between the phase diagrams of liquids with dynamical lines [10] and magnetic phase diagrams in the system of $Mn_{1-x}Fe_xSi$ solid solutions [52, 104]. However, phase diagrams of liquids are currently considered from the standpoint of changes in their structure under the influence of external conditions, and it remains unclear whether the change in the structure of short-range order in a liquid can be rightfully compared with the change in the regime of spin fluctuations in magnets.

In this paper, we essentially avoided the question of the possible classification of spin fluctuation phenomena by analogy with the division into first- and second-order transitions, crossovers, etc., as accepted in thermodynamics and statistical theory. The exception is the SFT to the spin nematic phase in CeB_6, where the heat capacity data correspond to a first-order phase transition. The reason for this omission is obvious, and it lies in the absence of models based on the expansion of the thermodynamic potential in the order parameter(s) that would specifically describe the SFTs, and not just the transitions between different magnetic structures. Based on the extensive methodological groundwork available in Landau's theory of phase transitions, we can expect that its generalization to the case of SFTs will be fruitful and will bring about answers to many questions in the physics of spin fluctuations that currently remain unanswered.

Acknowledgments

I sincerely thank K M Salikhov and A K Zvezdin for the useful discussions that took place during talks on the subject of this review. I express my deep gratitude to my wife Elena, without whose daily support this review would not have been written.

References

1. Vonsovskii S V *Magnetism* (New York: J. Wiley, 1974); Translated from Russian: *Magnetizm*: *Magnitnye Svoistva Dia-, Para-, Ferro-, Antiferro- i Ferrimagnetikov* (Moscow: Nauka, 1971)
2. Landau L D, Lifshitz E M *Statistical Physics* Vol. 1 (Oxford: Pergamon Press, 1980); Translated from Russian: *Statisticheskaya Fizika* Pt. I (Moscow: Nauka, 1976)
3. Tolédano J C, Tolédano P *The Landau Theory of Phase Transitions* (Singapore: World Scientific, 1987) https://doi.org/10.1142/0215
4. Anisimov M A, Gorodetskii E E, Zaprudskii V M *Sov. Phys. Usp.* **24** 57 (1981); *Usp. Fiz. Nauk* **133** 103 (1981)
5. Fleury P A *Science* **211** 125 (1981); Translated into Russian: *Usp. Fiz. Nauk* **138** 129 (1982)
6. Feynman R P *Statistical Mechanics* (Reading, MA: W.A. Benjamin, 1972); Translated into Russian: *Statisticheskaya Mekhanika* (Moscow: Mir, 1978)
7. Kvasnikov I A *Molekulyarnaya Fizika* (Molecular Physics) (Moscow: Editorial URSS, 2011)
8. Brazhkin V V *Phys. Usp.* **64** 1049 (2021); *Usp. Fiz. Nauk* **191** 1107 (2021)
9. Brazhkin V V *Phys. Usp.* **49** 719 (2006); *Usp. Fiz. Nauk* **176** 745 (2006)
10. Brazhkin V V et al. *Phys. Usp.* **55** 1061 (2012); *Usp. Fiz. Nauk* **182** 1137 (2012)
11. Brazhkin V V *Phys. Usp.* **60** 954 (2017); *Usp. Fiz. Nauk* **187** 1028 (2017)
12. Pikin S A, Indenbom V L *Sov. Phys. Usp.* **21** 487 (1978); *Usp. Fiz. Nauk* **125** 251 (1978)
13. Blinov L M *Structure and Properties of Liquid Crystals* (Dordrecht: Springer, 2010); Blinov L M *Zhidkie Kristally*: *Struktura i Svoistva* (Moscow: Librokom, 2013)
14. Ma Sh *Modern Theory of Critical Phenomena* (Reading, MA: W.A. Benjamin, 1976); Translated into Russian: *Sovremennaya Teoriya Kriticheskikh Yavlenii* (Moscow: Mir, 1980)
15. Wilson K G "The renormalization group and critical phenomena: Nobel Lecture, 8 December 1982", in *Nobel Lectures, Physics 1981–1990* (Ed.-in-Charge T Frängsmyr, Ed. G Ekspong) (Singapore: World Scientific Publ. Co., 1993); Translated into Russian: *Usp. Fiz. Nauk* **141** 193 (1983); Wilson K G *Rev. Mod. Phys.* **55** 583 (1983)
16. Demishev S V et al. *Phys. Solid State* **43** 320 (2001); *Fiz. Tverd. Tela* **43** 307 (2001)
17. Demishev S V *Appl. Magn. Reson.* **51** 473 (2020)
18. Smirnov A I *Phys. Usp.* **59** 564 (2016); *Usp. Fiz. Nauk* **186** 633 (2016)
19. Stishov S M, Petrova A E *Phys. Usp.* **54** 1117 (2011); *Usp. Fiz. Nauk* **181** 1157 (2011)
20. Ryzhov V N et al. *Phys. Usp.* **60** 857 (2017); *Usp. Fiz. Nauk* **187** 921 (2017)

21. Demishev S V, Semeno A V, Ohta H *Appl. Magn. Reson.* **52** 379 (2021)
22. Moriya T *Spin Fluctuations in Itinerant Electron Magnetism* (Berlin: Springer-Verlag, 1985)
23. Kaul S N *J. Phys. Condens. Matter* **11** 7597 (1999)
24. Kaul S N *J. Phys. Condens. Matter* **17** 5595 (2005)
25. Demishev S V et al. *Phys. Rev. B* **85** 045131 (2012)
26. Beille J et al. *J. Magn. Magn. Mater.* **10** 265 (1979)
27. Motokawa M et al. *J. Magn. Magn. Mater.* **70** 245 (1987)
28. Demishev S V et al. *JETP Lett.* **93** 213 (2011); *Pis'ma Zh. Eksp. Teor. Fiz.* **93** 231 (2011)
29. Demishev S V, Ishchenko T V, Samarin A N *Low Temp. Phys.* **41** 971 (2015); *Fiz. Nizk. Temp.* **41** 1243 (2015)
30. Brandt N B, Kul'bachinskii V A *Kvazichastitsy v Fizike Kondensirovannogo Sostoyaniya* (Quasiparticles in Condensed Matter Physics) (Moscow: Fizmatlit, 2005) pp. 491–521
31. Val'kov V V et al. *Phys. Usp.* **64** 641 (2021); *Usp. Fiz. Nauk* **191** 673 (2021)
32. Abrikosov A A *Fundamentals of the Theory of Metals* (Mineola, NY: Dover Publ., 2017) p. 283; Translated from Russian: *Osnovy Teorii Metallov* (Moscow: Fizmatlit, 2010) p. 284
33. Stishov S M et al. *Phys. Rev. B* **76** 052405 (2007)
34. Urbano R R et al. *Phys. Rev. B* **70** 140401 (2004)
35. Cooley J C et al. *Phys. Rev. B* **56** 14541 (1997)
36. Corti M et al. *Phys. Rev. B* **75** 115111 (2007)
37. Demishev S V et al. *JETP Lett.* **115** 673 (2022); *Pis'ma Zh. Eksp. Teor. Fiz.* **115** 717 (2022)
38. Brazovskii S A *Sov. Phys. JETP* **41** 85 (1975); *Zh. Eksp. Teor. Fiz.* **68** 175 (1975)
39. Janoschek M et al. *Phys. Rev. B* **87** 134407 (2013)
40. Brazovskii S A, Dmitriev S G *Sov. Phys. JETP* **42** 497 (1975); *Zh. Eksp. Teor. Fiz.* **69** 979 (1975)
41. Brazovskii S A, Filev V M *Sov. Phys. JETP* **48** 573 (1978); *Zh. Eksp. Teor. Fiz.* **75** 1140 (1978)
42. Fradkin E et al. *Annu. Rev. Condens. Matter Phys.* **1** 153 (2010)
43. Chu J-H et al. *Science* **329** 824 (2010)
44. Fernandes R M, Chubukov A V, Schmalian J *Nat. Phys.* **10** 97 (2014)
45. Penc K, Läuchli A M, in *Introduction to Frustrated Magnetism* (Springer Series in Solid-State Sciences, Vol. 164, Eds C Lacroix, F Mila, P Mendels) (Berlin: Springer, 2011) p. 331
46. Nikolaev A V, Tsvyashchenko A V *Phys. Usp.* **55** 657 (2012); *Usp. Fiz. Nauk* **182** 701 (2012)
47. Bogoslovskiy N A, Petrov P V, Averkiev N S *JETP Lett.* **114** 347 (2021); *Pis'ma Zh. Eksp. Teor. Fiz.* **114** 383 (2021)
48. Bhatt R N, Lee P A *Phys. Rev. Lett.* **48** 344 (1982)
49. Demishev S V et al. *JETP Lett.* **98** 829 (2014); *Pis'ma Zh. Eksp. Teor. Fiz.* **98** 933 (2013)
50. Sachdev S *Quantum Phase Transitions* 2nd ed. (Cambridge: Cambridge Univ. Press, 2011)
51. Shklovskii B I, Efros A L *Electronic Properties of Doped Semiconductors* (Berlin: Springer-Verlag, 1984); Translated from Russian: *Elektronnye Svoistva Legirovannykh Poluprovodnikov* (Moscow: Nauka, 1979)
52. Demishev S V et al. *JETP Lett.* **103** 321 (2016); *Pis'ma Zh. Eksp. Teor. Fiz.* **103** 365 (2016)
53. Grigoriev S V et al. *Phys. Rev. B* **83** 224411 (2011)
54. Abrahams E, Wölfle P *Phys. Rev. B* **78** 104423 (2008)
55. Wölfle P, Abrahams E *Phys. Rev. B* **80** 235112 (2009)
56. Schlottmann P *Phys. Rev. B* **79** 045104 (2009)
57. Demishev S V *Dokl. Phys.* **66** 187 (2021); *Dokl. Ross. Akad. Nauk. Fiz. Tekh. Nauki* **499** (1) 3 (2021)
58. Demishev S V, in *Nanofizika i Nanoelektronika. Trudy XXVII Mezhdunarodnogo Simpoziuma, Nizhnii Novgorod, 13–16 Marta 2023 g.* (Nanophysics and Nanoelectronics. Proc. of the XXVII Intern. Symp., Nizhny Novgorod, 13–16 March 2023) Vol. 1 (Nizhny Novgorod: IPF RAN, 2023) p. 181
59. Effantin J M et al. *J. Magn. Magn. Mater.* **47–48** 145 (1985)
60. Nakao H et al. *J. Phys. Soc. Jpn.* **70** 1857 (2001)
61. Lee K N, Bell B *Phys. Rev. B* **6** 1032 (1972)
62. Takigawa M et al. *J. Phys. Soc. Jpn.* **52** 728 (1983)
63. Kawakami M et al. *Solid State Commun.* **36** 435 (1980)
64. Hall D, Fisk Z, Goodrich R G *Phys. Rev. B* **62** 84 (2000)
65. Takase A et al. *Solid State Commun.* **36** 461 (1980)
66. Sakai O et al. *J. Phys. Soc. Jpn.* **66** 3005 (1997)
67. Shina R, Shiba H, Thalmeier P *J. Phys. Soc. Jpn.* **66** 1741 (1997)
68. Sera M, Kobayashi S *J. Phys. Soc. Jpn.* **68** 1664 (1999)
69. Tsuji S, Sera M, Kojima K *J. Phys. Soc. Jpn.* **70** 41 (2001)
70. Tsuji S, Sera M, Kojima K *J. Phys. Soc. Jpn.* **70** 2864 (2001)
71. Hanzawa K, Kasuya T *J. Phys. Soc. Jpn.* **53** 1809 (1984)
72. Hanzawa K *J. Phys. Soc. Jpn.* **73** 1228 (2004)
73. Murakami Y et al. *Phys. Rev. Lett.* **80** 1932 (1998)
74. Khomskii D I *Int. J. Mod. Phys. B* **15** 2665 (2001)
75. Ivannikov D et al. *Phys. Rev. B* **65** 214442 (2002)
76. Semeno A V, Okubo S, Ohta H, Demishev S V *Appl. Magn. Reson.* **52** 459 (2021)
77. Semeno A V et al. *Sci. Rep.* **6** 39196 (2016)
78. Demishev S V et al. *Sci. Rep.* **7** 17430 (2017)
79. Sluchanko N E et al. *J. Exp. Theor. Phys.* **104** 120 (2007); *Zh. Eksp. Teor. Fiz.* **131** 133 (2007)
80. Zabrodskii A G et al. *Appl. Magn. Reson.* **35** 439 (2009)
81. Zabrodskii A, Veinger A, Semenikhin P *Appl. Magn. Reson.* **51** 327 (2020)
82. Zabrodskii A G *JETP Lett.* **33** 243 (1981); *Pis'ma Zh. Eksp. Teor. Fiz.* **33** 258 (1981)
83. Poklonski N A et al. *AIP Adv.* **11** 055016 (2021)
84. Poklonskaya O N *Vestn. Beloruss. Gos. Univ. Ser. 1 Fiz. Matem. Inform.* (2) 60 (2013)
85. Veinger A I et al. *JETP Lett.* **115** 685 (2022); *Pis'ma Zh. Eksp. Teor. Fiz.* **115** 730 (2022)
86. Shestakov A V et al. *IEEE Magn. Lett.* **11** 2503505 (2020)
87. Stepniewski R *Solid State Commun.* **58** 19 (1986)
88. Demishev S V *Dokl. Phys.* **67** 410 (2022); *Dokl. Ross. Akad. Nauk. Fiz. Tekh. Nauki* **506** (2) 40 (2022)
89. Yu U, Min B I *Phys. Rev. B* **74** 094413 (2006)
90. Bauer A et al. *Phys. Rev. B* **82** 064404 (2010)
91. Bauer A, Pfleiderer C *Phys. Rev. B* **85** 214418 (2012)
92. Demishev S V et al. *Phys. Usp.* **59** 559 (2016); *Usp. Fiz. Nauk* **186** 628 (2016)
93. Glushkov V V et al. *Phys. Rev. Lett.* **115** 256601 (2015)
94. Griffiths R B *Phys. Rev. Lett.* **23** 17 (1969)
95. Bray A J *Phys. Rev. Lett.* **59** 586 (1987)
96. Demishev S V et al. *JETP Lett.* **100** 28 (2014); *Pis'ma Zh. Eksp. Teor. Fiz.* **100** 30 (2014)
97. Lobanova I I, Glushkov V V, Sluchanko N E, Demishev S V *Sci. Rep.* **6** 22101 (2016)
98. Kittel Ch *Introduction to Solid State Physics* (New York: Wiley, 1971); Translated into Russian: *Vvedenie v Fiziku Tverdogo Tela* (Moscow: Nauka, 1978) p. 606
99. Mena F P et al. *Phys. Rev. B* **67** 241101 (2003)
100. Wangsness R K *Phys. Rev.* **91** 1085 (1953)
101. Dorfman Ya G *Magnitnye Svoistva i Stroenie Veshchestva* (Magnetic Properties and Structure of Matter) (Moscow: Gostekhizdat, 1955); Dorfman Ya G *Magnitnye Svoistva i Stroenie Veshchestva* (Magnetic Properties and Structure of Matter) 2nd ed., rev. (Moscow: LKI, 2010)
102. Demishev S V et al. *Sci. Rep.* **8** 7125 (2018)
103. Tanaka H *J. Chem. Phys.* **153** 130901 (2020)
104. Demishev S V et al. *JETP Lett.* **104** 116 (2016); *Pis'ma Zh. Eksp. Teor. Fiz.* **104** 113 (2016)